Permeability Characterization of Fiber Reinforcements Used in Liquid Composite Molding

by

Hasan Çağlar

A Dissertation Submitted to the
Graduate School of Sciences and Engineering
in Partial Fulfillment of the Requirements for
the Degree of

Master of Science
in
Mechanical Engineering

KOÇ UNIVERSITY

July 2018

Permeability Characterization of Fiber Reinforcements Used in Liquid Composite Molding

Koç University

Graduate School of Sciences and Engineering

This is to certify that I have examined this copy of a master's thesis by

Hasan Çağlar

and have found that it is complete and satisfactory in all respects,

and that any and all revisions required by the final

examining committee have been made.

Committee Members:

____

E. Murat Sözer, Ph.D. (Advisor)

____

Melis Şerefoğlu, Ph.D.

____

Hatice Sinem Şaş Çaycı, Ph.D.

ABSTRACT

Experimental setups were designed and constructed to characterize permeability of fabric preforms used in liquid composite molding processes for three different flow dimensions (linear, radial and through-thickness). They allow measuring both unsaturated and saturated permeabilities in linear and radial flows, but only steady (saturated) permeability in through-thickness direction. Four common curve fitting methods (global, single-step, reference time step, elementary methods) are used to fit the analytically expected formulas that are driven from Darcy's Law and conservation of mass experimental data. It is investigated how closely these four curve fitting methods fit to the experimental data by comparing their R-squared values. In agreement with the previous literature, in general there is a very significant variation between the results of the repeated experiments due to inherent variations in the material used and labor of fabric cutting, stacking and placement in the mold. This study contributes to the composite research by investigating which setups, conditions and curve-fitting method are more suitable to model the resin flow through fabric preforms used in Liquid Composite Molding (LCM), and also help decreasing the mentioned variation in 1D and 2D permeability measurements.

ÖZET

İki eksenli E-cam elyaf dokumanın üç farklı akış boyutunda (doğrusal, radyal ve kalınlık yönünde) geçirgenliğinin karakterize edilmesi için deney düzenekleri tasarlandı ve imal edildi. Bu deney düzenekleri, doğrusal ve radyal akışlarda kararsız ve kararlı geçirgenlik ölçümlerini, kalınlık yönünde ise sadece kararlı geçirgenlik ölçümüne uygundur. Dört yaygın eğri oturtma metodu (tüm veri, tek adım, referans zaman adımı, basit metodları), Darcy ve kütle korunumu kanunlarından elde edilen analitik denklemlerin deney verilerine oturtulması için kullanılacaktır. R-kare değerleri kıyaslanarak, bu metodların deney sonuçlarına ne kadar iyi uyduğu incelenecektir. Literatüre mutabık şekilde, kullanılan malzemedeki ve dokumanın kesim, istiflenme ve yerleştirilme işçiliğindeki farklılıklardan dolayı, tekrarlanan geçirgenlik deney sonuçlarında belirgin farklılıklar vardır. Bu çalışmanın kompozit araştırmalarına katkısı, hangi geçirgenlik ölçüm deney düzeneği, koşulları ve eğri oturtma metodunun, Sıvı Kompozit Kalıplama üretim yöntemindeki reçine akışının modellenmesinde kullanılmasının uygun olduğunu belgelendirmeyi ve bahsedilen geçirgenlik ölçümündeki farklılıkların azaltılmasıdır.

ACKNOWLEDGEMENTS

I would like to thank my advisor Prof. E. Murat Sözer for his support, patience and guidance at every stage of my graduate study. I would like to thank members of my thesis committee Prof. Melis Şerefoğlu and Prof. Hatice Sinem Şaş Çaycı for their participation with insightful comments.

I would also like to thank to the staff of Graduate School of Sciences and Engineering and College of Engineering for their support and patience.

I owe my gratitude to Dr. Barış Çağlar for his positive influences on my life in every aspect. I would like to thank my colleagues, Dr. Mehmet Akif Yalçınkaya, Mert Hancıoğlu, Serhan Enes Kalmış and Berkay Terzi for their support.

I am thankful to Tayyip Adal, Burak Baran Kula, Emre Tıraşçı, Berker Kantar, Sercan Göğerçin, Ziya Subaşı, Mahmut Biçer and Ömer Şirin for their supportive friendships and also my cousins Umut Aksu and Hasan Girdap.

My deepest gratitude is to my father Ferhat, my mother Ruhan, my sister Dilek, my brother-in-law Fatih, my niece Elif, my older brother Barış and his fiancée Büşra, my sister Nuran and her fiancé Uygur for their support, patience and worthless love.

TABLE OF CONTENTS

LIST OF FIGURES

LIST OF TABLES

Chapter 1
INTRODUCTION

A composite material is made from at least two different materials, and it exhibits distinct and more favorable properties compared to the properties of its constituents. Majority of the fiber reinforced polymer composites manufactured by any one of Liquid Composite Molding (LCM) processes contain a cured thermoset polymer (matrix component) which surrounds a fiber structure (reinforcing component). The polymer resin is either thermoset or thermoplastic, but it is almost always thermoset in LCM due to its lower viscosity than thermoplastics. The polymeric component provides the followings: (1) keeping the fibers at a fixed configuration (note that fibers alone are loose and cured polymer matrix gives the final shape of the composite material), (2) compressive and shear strength (although fibers are strong under tension, they do not support compressive loading), and (3) environmental durability (such as resistance to humidity and sunlight). The reinforcement fibers (commonly glass, carbon or Kevlar) have the following major functions: (1) major contribution to support structural load on the composite part, (2) decrease thermal stresses on the material, and (3) achieve high specific stiffness and strength (i.e., these overall mechanical properties divided by the overall density of the final composite material) on the macroscopic level compared to many metal alternatives [1].

Fiber reinforced polymer composites are preferred in aerospace, automotive and infrastructure industries due to their high performance (high mechanical properties such as strength and stiffness) and lightweight compared to metals typically used in these industries. However, manufacturing of composite materials is neither repeatable nor completely standardized especially compared to metals. The variability of the materials and non-repeatable labor (fabric cutting, stacking and placement in the mold cavity) and non-uniform fiber structure affect properties of the final product which typically have an inherent and significant variation not only in a single part, but also among the parts manufactured. This is an important issue especially when the tight tolerances (in dimensions, physical and mechanical properties) required in aerospace and automotive industries are considered. However, researches on composite materials aim to make these variations smaller with the help of new manufacturing technology and process modeling that allow engineers to design appropriate process parameters (such as injection conditions, selection of material, mold configuration and so on) [2].

1.1. Liquid Composite Molding Process (LCM)

LCM is the family of composite processing techniques in which a dry fabric preform placed in the mold cavity is impregnated with the liquid thermoset resin driven into the mold by means of an applied pressure differential between the inlet and exit gates.

The main steps of LCM processes are as follows. Dry fabric layers are cut to desired dimensions and draped over a lower mold half (or draped over a tool with the same shape and then transferred to the lower mold half). The mold is closed to desired thickness. The compacted preform is impregnated with liquid resin by opening the inlet gate. After complete mold filling and continuing resin flushing for a while, the inlet and exit gates are closed. The part is kept in the mold until the resin is partially cured (either at room temperature or at elevated temperature depending on the resin system used) and becomes rigid enough so that no significant warpage occurs during demolding. After demolding and complete curing, the part is trimmed to the final shape.

The two most common LCM processes are Resin Transfer Molding (RTM) and Vacuum Assisted Resin Transfer Molding (VARTM). The steps of these two processes are demonstrated in Fig. 1.1 and Fig. 1.2, respectively.

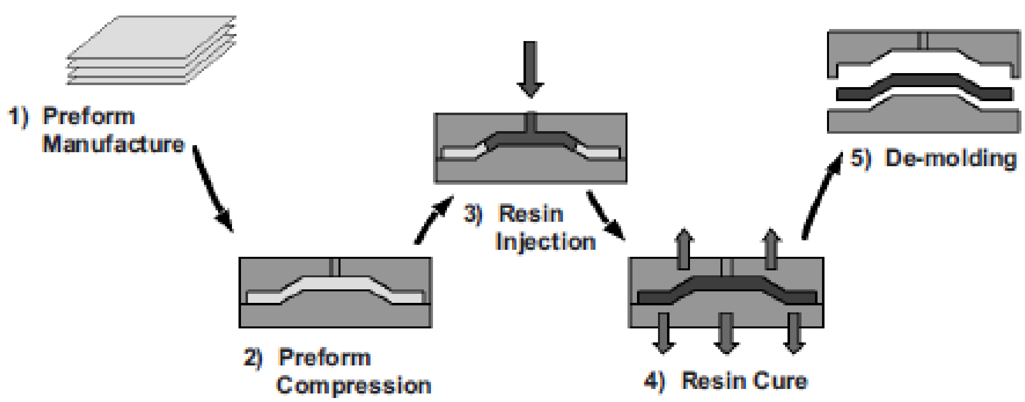

Figure 1.1 Schematic of the steps of RTM process [1].

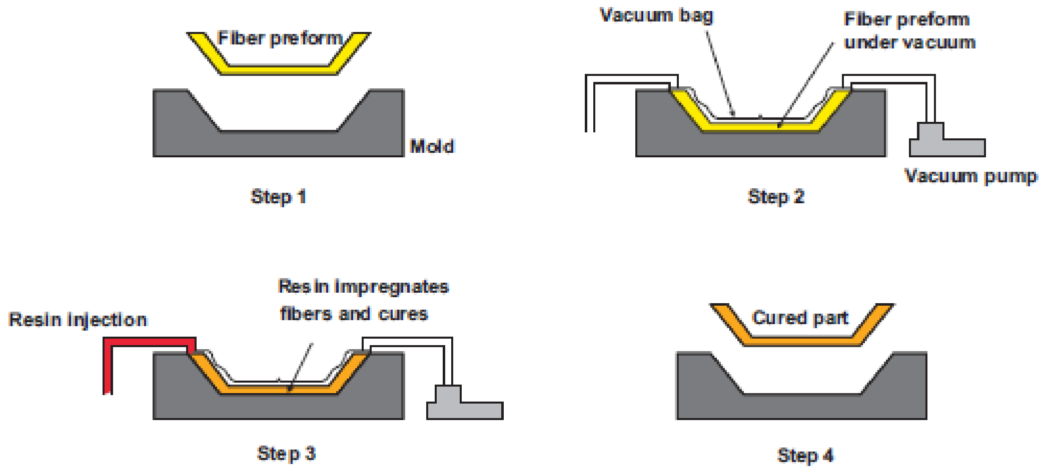

Figure 1.2 Schematic of the steps of VARTM process [1].

The main distinction between RTM and VARTM processes is that a two-sided rigid mold is used in RTM whereas one-sided rigid mold is used in VARTM process (flexible vacuum bag and tacky tape are used to create mold cavity and seal it). Thus, this vacuum bag becomes the upper mold half in VARTM. Usually positive pressure injection is created in RTM by using an injection machine at the inlet gate, whereas vacuum pressure is generated in the mold of VARTM by using a vacuum pump connected to the exit. Resin reservoir in VARTM is open to atmosphere.

The RTM process offers several benefits: (1) near net shape manufacturing of composite materials, (2) achieving higher fiber volume fractions (up to 65-70 %) enabling to achieve superior mechanical properties, (3) production of materials with good dimensional tolerance and surface finish on both faces owing to the two-sided rigid molds. On the other hand, the main issues of RTM can be listed as: (1) high initial investment requirements due to an injection machine and two-sided molds with small dimensional tolerances (this is very challenging task when the two matching surfaces are considered), and (2) requirement of clamping equipment or press suitable for high injection pressure and thus can apply enough force to close the mold.

VARTM offers several advantages compared to RTM process: (1) lower investment on the mold, (2) simpler system for mold closure and fluid infusion, (3) ability to track the resin flow propagation during the process due to transparent upper mold half which is a special nylon bag, (4) manufacturing of complex and large parts (wind turbine blades and boat hulls can be in the order of tens of meters). On the other hand, there are some drawbacks in VARTM process: (1) poor dimensional tolerances especially in the thickness direction and thickness variation within the produced parts due to flexible vacuum bag, (2) long mold fill times due to limited pressure differential between the inlet and exit gates (which is one atmospheric pressure or less), and (3) inability to achieve high fiber volume fractions due to the mentioned limited pressure differential which also determines the maximum level of compaction pressure applied on a fabric preform [3].

1.2. Permeability

More than a century ago, Henry Darcy observed that the flow rate through a sand/rock bed was linearly proportional to pressure gradient and inversely proportional to the viscosity of the liquid (water). His empirical formulation, which is known as Darcy's Law, is commonly used for modeling porous media flows. For one-dimensional flows (see Fig. 1.3), Darcy's Law is given as follows [1]:

$$\bar{u} = \frac{Q}{A} = -\frac{K}{\mu}\frac{dP}{dx} \tag{1.1}$$

where $\bar{u}$ is the resin velocity (a.k.a. the volume averaged Darcy's velocity), Q is the volumetric flow rate, dP/dx is the pressure gradient in liquid, K is the permeability of the porous medium (which is the sand/rock bed) along the flow direction, and μ (shown as η in that figure) is the liquid viscosity [1].

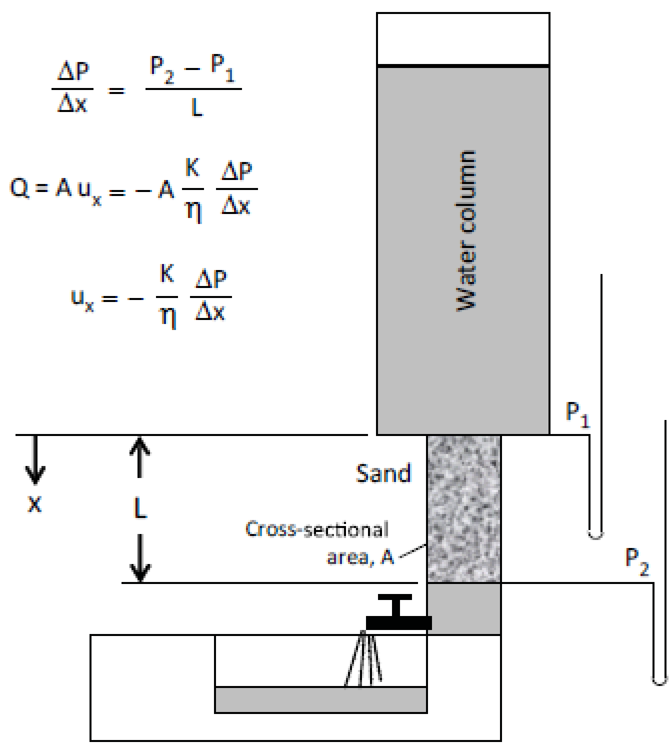

Figure 1.3 Darcy used a column of sand to measure the permeability of the sand [1].

Permeability of a fabric preform indicates how easy a fluid flows through the pores of the fabric preform. That means, permeability is the inverse of the resistance to the flow. Permeability characterization can be carried out by performing experiments under certain boundary conditions. Permeability is determined by fitting numerical or analytical solution of the Darcy's Law to the experimental data where the other parameters (viscosity and boundary conditions) are fixed in both experiments and model.

Flow simulations based on Darcy's Law are used for modeling resin flow through porous fabric preforms used in LCM. These simulations allow designing and selection of process parameter window such as pressure or flow rate at inlet and outlet, scheduling the boundary conditions (i.e., when inlet and/or outlet should be opened or closed) to optimize one or both of the following: (a) shorten mold filling time, and (b) minimize or ideally avoid any void (a.k.a. dry spots).

For higher dimensional flows (2D or 3D) than 1D, Darcy's Law takes the following form:

$$\bar{u} = -\frac{[K]}{\mu} \circ \nabla P \tag{1.2}$$

where ∇P is the resin pressure gradient and $[K]$ is the permeability tensor of the porous medium [1].

Solving the conservation of momentum in the porous network of empty channels of a typical fabric preform used in LCM is very challenging and almost an impossible task due to the complexity of modeling and generating this complicated channel network. Instead of this approach, Darcy's Law (which is the macroscopic and empirical relationship between the resin velocity (and thus flow rate) and the pressure gradient) is solved for the resin flow that takes place during the mold filling of composite manufacturing processes [1].

Fabric preforms with anisotropic structure have different permeability components in three orthogonal directions [1]:

$$[K] = \begin{bmatrix} K_{xx} & K_{xy} & K_{xz} \\ K_{yx} & K_{yy} & K_{yz} \\ K_{zx} & K_{zy} & K_{zz} \end{bmatrix} \tag{1.3}$$

Eq. (1.2) can be expressed in matrix form as follows:

$$\begin{pmatrix} \bar{u}_x \\ \bar{u}_y \\ \bar{u}_z \end{pmatrix} = -\frac{1}{\mu} \begin{bmatrix} K_{xx} & K_{xy} & K_{xz} \\ K_{yx} & K_{yy} & K_{yz} \\ K_{zx} & K_{zy} & K_{zz} \end{bmatrix} \circ \begin{pmatrix} \partial P/\partial x \\ \partial P/\partial y \\ \partial P/\partial z \end{pmatrix} \tag{1.4}$$

Assuming $K_{ij} = K_{ji}$, only six scalar components are needed to obtain the full permeability tensor. If the principal directions of the fabric preform are selected as x-, y- and z-axes, Eq. (1.4) can be written as

$$\begin{pmatrix} \bar{u}_x \\ \bar{u}_y \\ \bar{u}_z \end{pmatrix} = -\frac{1}{\mu} \begin{bmatrix} K_{xx} & 0 & 0 \\ 0 & K_{yy} & 0 \\ 0 & 0 & K_{zz} \end{bmatrix} \begin{pmatrix} \partial P/\partial x \\ \partial P/\partial y \\ \partial P/\partial z \end{pmatrix} \tag{1.5}$$

To characterize the unsaturated and saturated permeabilities in the principal directions, there are three different experimental methods: (1) one-dimensional (a.k.a. linear) in-plane flow along each of the two in-plane directions, (2) alternative to a set of two experiments mentioned in the previous approach, a two-dimensional (a.k.a. radial) in-plane flow from a central injection hole, and (3) three dimensional (hemispherical) flow or simply 1D flow along through-thickness direction by adjusting that z-axis is the thickness direction [1].

In most cases, the in-plane permeability measurements are sufficient (that means no need to measure the permeability along out-of-plane direction (a.k.a. through-thickness direction)) because the thickness of the fabric preform is negligible in comparison with the in-plane dimensions of the fabric and the flow is assumed to be 2D in the in-plane directions. Note that resin flow in the shell-like mold cavity in 3D can still be modeled as 2D as long as the permeability tensor is measured in the planar axes of the shell.

In this study, permeability of a fabric preform is characterized for both unsaturated and saturated 1D (linear) flow regimes under constant-injection pressure boundary condition [4] as it will be detailed in Chapter 2.

In addition, 2D (radial) unsteady permeability under constant-injection pressure boundary condition is measured [5] as it will be detailed in Chapter 2.

The radial resin flow is modeled and solved numerically to obtain 2D steady permeability of the fabric preform along both principal axes, as it will be exemplified in Chapter 5.

The main contributions of this thesis are (1) designing and constructing three permeability characterization setups (linear, radial and through-thickness), and (2) conduct permeability measurements under different flow regimes (unsaturated and saturated) and different dimensions (1D and 2D), obtain the results by using different curve fitting models and then compare them. As previously investigated [6],6], in general there is a very significant variation between the results of the repeated experiments done in the same study due to aforementioned and inherent variations in the material used and labor. The variation is very common and can be several orders of magnitude among different institutes and laboratories [5,6]. This current study aims to document which setups, conditions and/or curve-fitting model are more suitable to model the resin flow through fabric preforms used in LCM, and also help decreasing the mentioned variation in permeability measurements.

Chapter 2
PERMEABILITY MEASUREMENT

Different types of permeability measurement experiments are described in this chapter. The permeability measurement experiments are classified by

- the flow direction (1D or 2D both in-plane, or through-thickness direction which is out-of-plane),
- the flow regime (unsteady or steady),
- the injection boundary condition used (constant-injection pressure or constant-injection flow rate).

In this study, all subclasses of the first two main class experiments (i.e., all flow dimensions and both flow regimes) are conducted under constant-injection pressure boundary condition.

The permeability of a fabric preform in through-thickness direction (a.k.a. z-direction) is called through-thickness permeability. This permeability is usually several orders of magnitude smaller than the in-plane permeability components due to the porous structure of fabric preform.In this study, both 1D (linear) permeability and 2D (radial) permeability are measured under both unsteady (a.k.a. unsaturated permeability) and steady flow regimes (a.k.a. saturated permeability). Through-thickness permeability measurements are performed under steady flow conditions because tracking the flow front propagation requires transparent parts or use of sensors, which are difficult to have in the small mold cavity because of the concerns related to enough rigidity or disturbance of the resin flow.

For both in-plane permeability measurement types (linear and radial), a dry fabric preform (stacked layers of a fabric cut to desired in-plane dimensions) is placed in the mold cavity. A rectangular preform and a square preform with a central hole are used in 1D and radial flow experiments, respectively (see Chapter 3 for details). Constant-pressure boundary condition is used in all experiments. This is satisfied by keeping the inlet resin reservoir open to atmosphere and connecting a resin trap and a vacuum pump to the exit. The vacuum level is kept constant in all experiments. Once the vacuum level is set and then the inlet gate is opened, first, the unsteady permeability is measured by tracking the position of the flow front over time in the post-processing of the video record. For tracking purpose, sensor data (such as pressure sensors signaling resin arrival times to specific locations) could be used alternative to videos as described by Yalcinkaya et al. [8].

In this study, the videos are post-processed to determine $x_f(t)$ versus t in 1D experiment, $r_0(t)$ and $r_{90}(t)$ versus t in the radial experiment. Here $x_f(t)$ is the flow front position in 1D, r_0(t) and $r_{90}(t)$ are the major and minor radii of the elliptical flow front in the 2D radial flow.

After resin arrives to the exit and enough time elapses so that the fabric preform is saturated completely, the steady permeability measurement experiment is continued by using the same fabric specimen and boundary conditions. That means, resin injection is continued by keeping the inlet and exit open, and either the mass of the resin in the reservoir or the mass of the resin coming out of the mold is recorded by using a digital scale to calculate flow rate indirectly [8]. The detail will be given below.

2.1. 1D Permeability Measurement Experiments under Constant-Injection Pressure Boundary Condition

In 1D permeability measurement experiments, the constant pressure difference between inlet and exit provides the resin propagation in the mold cavity [3].

1D unsteady permeability (K_{uns}) of a fabric preform under constant-injection pressure is calculated by using the following equation [3]:

$$K_{uns} = \frac{C\,\mu\,\phi}{2\,\Delta P} \tag{2.1}$$

where μ is the viscosity of the resin, ϕ is the porosity of the fabric preform (which is equal to $1 - V_f$), ΔP is the pressure differential between the inlet and exit (in this case, it is equal to the vacuum pressure applied by the vacuum pump, since the inlet is open to atmosphere) and C is calculated by post-processing the flow front position versus time data. For a 1D flow under constant-pressure boundary condition and through a constant mold gap thickness, Darcy's Law yields that

$$x_f(t) = \sqrt{\frac{2K\Delta P\,t}{\mu(1-V_f)}} = \sqrt{C\,t} \tag{2.2}$$

Eq. (2.2) is best-fit to the experimentally observed flow front position $x_f(t)$ to determine C. A least squares method is used to minimize the error between the experimental data and the curve fit.

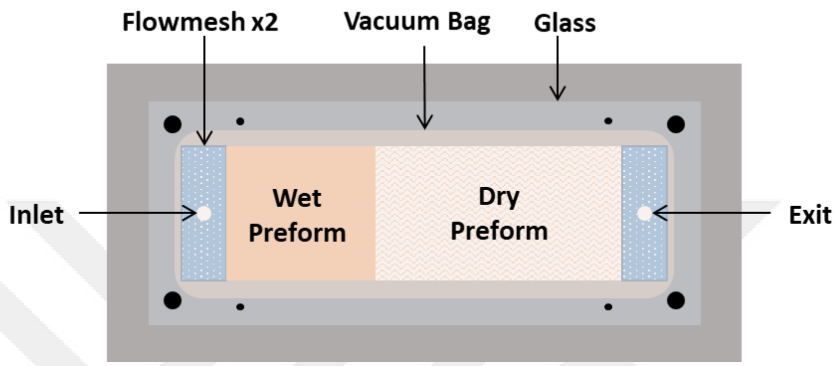

Figure 2.1 The thickness distribution in the 1D experimental setup (a) before resin infusing (b) during resin impregnating through the mold cavity.

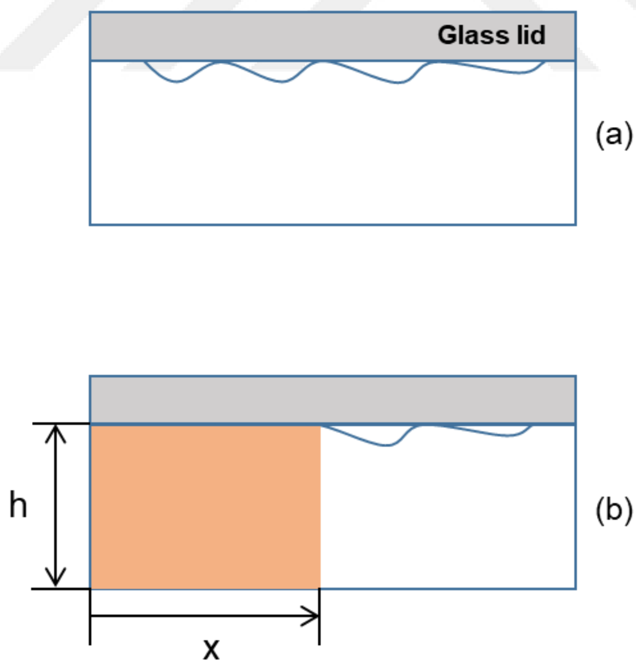

Figure 2.2 The thickness distribution in the 1D experimental setup (a) before resin infusing (b) during resin impregnating through the mold cavity.

The glass lid seen in Fig. 2.1 is used to convert the VARTM experimental setup to a RTM setup by simply setting the mold cavity thickness to a fixed value. One could raise a question because the fabric preform may have some thinner regions as shown in Fig. 2.2 (a) than the set value. However, notice that when resin arrives these thinner regions, it is thickened as shown Fig. 2.2 (b) due to increased resin pressure ans thus decreased compaction pressure on the vacuum bag and fabric preform. Therefore, the setup behaves as a constant mold cavity thickness after the specimen is wetted [9].

Once the resin impregnates the fabric preform completely and reaches the exit, the unsteady permeability measurement experiment is finished, however the resin infusion is continued by keeping the gate and exit open. In this second part, steady permeability measurement experiment is conducted in which steady flow rate is needed. Mass of the resin, m, in the inlet reservoir is measured over time. The mass flow rate $\dot{m}$ is the negative slope of mass versus time curve, dm/dt. $\dot{m}$ divided by the density of the resin ρ, volumetric flow rate Q is calculated to substitute in 1D steady permeability (K_s) formula [3]:

$$K_s = \frac{Q\ \mu\ L}{w\ h\ \Delta P} = \frac{\dot{m}\ \mu\ L}{\rho\ w\ h\ \Delta P} \tag{2.3}$$

where L, w, h are length, width and thickness of the fabric preform, respectively [3].

2.2. 2D Radial Permeability Measurement Experiments under Constant-Injection Pressure Boundary Condition

In 2D (radial) permeability measurement experiments, the resin is infused from the center of the lower mold by using pressurized air in the resin inlet pot and a pressure regulator; the outlet vent is kept open to atmosphere.

The center of fabric layers is punched to make an inlet hole, and the punch diameter is equal to the inlet diameter so that it prevents the resin flow through thickness direction of the fabric when it first enters the mold cavity (see Chapter 3 for details).

The resin flow front propagates either as a circle for isotropic fabric preforms, or as an ellipse for anisotropic fabric preforms. In other words, if an isotropic fabric preform is used, the permeability values in principal directions, $R_{0^o}(t)$ and $R_{90^o}(t)$, should be equal to each other.

In this study, an anisotropic biaxial fabric preform is used in the experiments as will be detailed in Chapters 3 and 4.

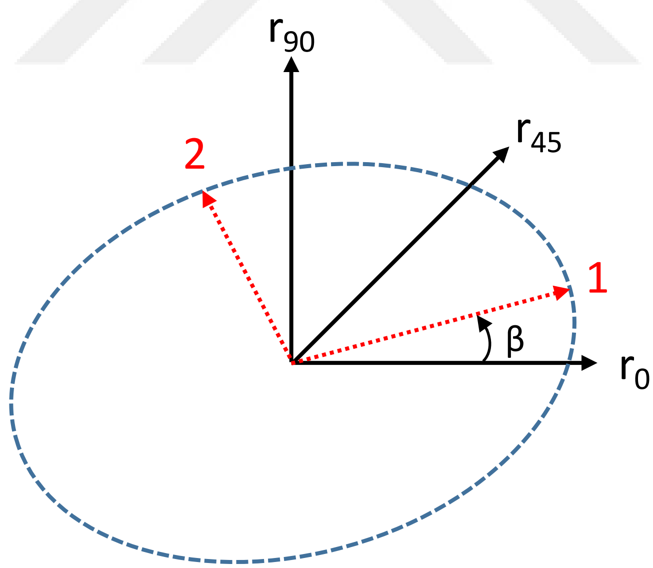

Figure 2.3 In-plane flow front propagation through an anisotropic fabric preform.

$R_{0^o}(t)$ is the flow front radius along the production line of a fabric roll, and $R_{90^o}(t)$ is the flow front radius along the transverse direction (i.e., along the width of the roll). In general, the resin flows faster along the production direction

(0^o) of the fabric preform than along the 90^o degree direction as depicted in Fig. 2.1. This is due to the fact that porosity is higher along the 0^o direction than 90^o direction for the fabric used (see the detail in Chapter 3). In our study, β was measured to be small so that 0^o and 90^o directions will be treated as the principal directions (see Chapter 5).

Compared to an unsteady 1D permeability measurement experiment, an unsteady 2D permeability measurement experiment is more advantageous due to: (1) it allows to measure both in-plane principal permeabilities (or alternatively along 0^o and 90^o directions) in a single experiment, (2) therefore it is less time consuming, and (3) it is not subject to race-tracking that may take place between fabric boundaries and mold walls of a 1D experiment which causes deviation from 1D flow and making the permeability computations unreliable.

The flow front positions of both axes (R_{0^o} and R_{90^o}) are recorded during an experiment by using a digital camera placed over the mold.

2D (radial) unsteady permeability (K_{uns}) components along the production and transverse directions of a fabric preform under constant-injection pressure are calculated by using the following equations [5]:

$$K_{uns,0} = \frac{\mu\,\phi}{4P_{inj}}\left\{r_{f,0}^2\left(2\,ln\left(\frac{r_{f,0}}{r_i}\right)-1\right)+r_i^2\right\}\frac{1}{t} \qquad (2.4)$$

$$K_{uns,90} = \frac{\mu\,\phi}{4P_{inj}}\left\{r_{f,90}^2\left(2\,ln\left(\frac{r_{f,90}}{r_i}\right)-1\right)+r_i^2\right\}\frac{1}{t} \qquad (2.5)$$

where μ is the viscosity of the resin, ϕ is the porosity of the fabric preform, P_{inj} is the injection pressure at the inlet, r_f is the radius of the flow front (R_{0^o} and

R_{90^o} for the two directions), r_i is the radius of the inlet hole (0.006 m) and t is time.

Second part of the experiment (steady-state condition) is conducted after the fabric preform is fully impregnated with resin. In this part, the resin coming out of the eight outlets (see Fig. 2.2) is accumulated in the container and mass of the resin is measured over time by using a digital scale.

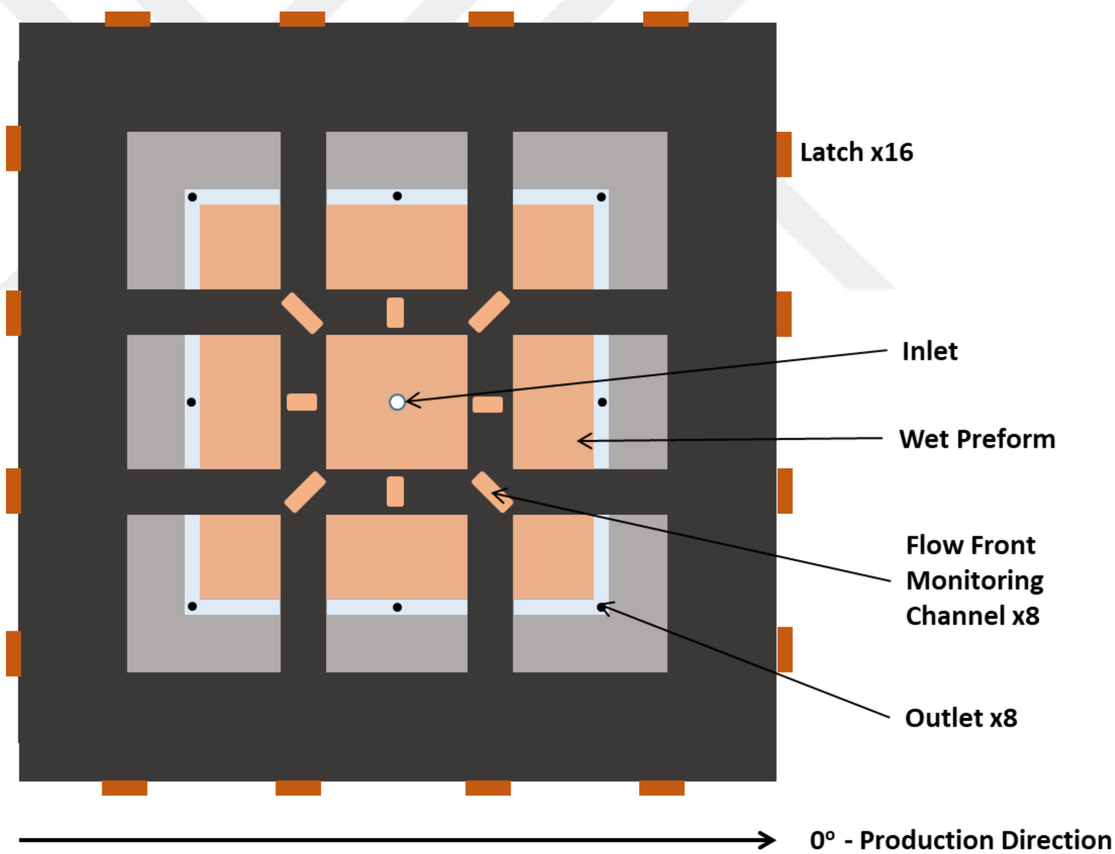

Figure 2.4 Top view of 2D (radial) permeability measurement setup with a steady flow regime (i.e. when the fabric preform is completely saturated).

Total mass flow rate $\dot{m}$ is the first order curve fit to the experimental data (cumulated mass collected in the container versus time) and it is divided by the density of the resin ρ to calculate the volumetric flow rate Q.

The total outflow volumetric flow rate is determined numerically and compared with the experimental volumetric flow rate to compute the steady permeability components for the two axes. For this purpose, conservation of mass is considered (see Fig. 2.3):

$$\left[\left(-\frac{K_{s,xx}}{\mu}\frac{\partial P}{\partial x}\right)_x - \left(-\frac{K_{s,xx}}{\mu}\frac{\partial P}{\partial x}\right)_{x+\Delta x}\right] h\,\Delta y + \left[\left(-\frac{K_{s,yy}}{\mu}\frac{\partial P}{\partial y}\right)_y - \left(-\frac{K_{s,yy}}{\mu}\frac{\partial P}{\partial y}\right)_{y+\Delta y}\right] h\,\Delta x = 0 \qquad (2.6)$$

Multiplying the first term on the left hand side with $\Delta x/\Delta x$ and the second term with $\Delta y/\Delta y$ and letting Δx and Δy approach to infinitesimal dx and dy results in the following differential equation:

$$\frac{K_{s,xx}}{\mu}\frac{\partial^2 P}{\partial x^2} + \frac{K_{s,yy}}{\mu}\frac{\partial^2 P}{\partial y^2} = 0 \qquad (2.7)$$

or simply,

$$\frac{K_{s,xx}}{K_{s,yy}}\frac{\partial^2 P}{\partial x^2} + \frac{\partial^2 P}{\partial y^2} = 0 \qquad (2.8)$$

Eq. 2.8 will be solved inside the resin-filled domain by using finite-differences, and the boundary conditions at the inlet hole and outer boundary conditions are shown in Fig. 2.3.

It is assumed that the ratio of the unsteady permeability components is the same as the ratio of the unsteady permeability components that were already found in the unsteady permeability characterization:

$$\frac{K_{s,xx}}{K_{s,yy}} = \frac{K_{uns,xx}}{K_{uns,yy}} \tag{2.9}$$

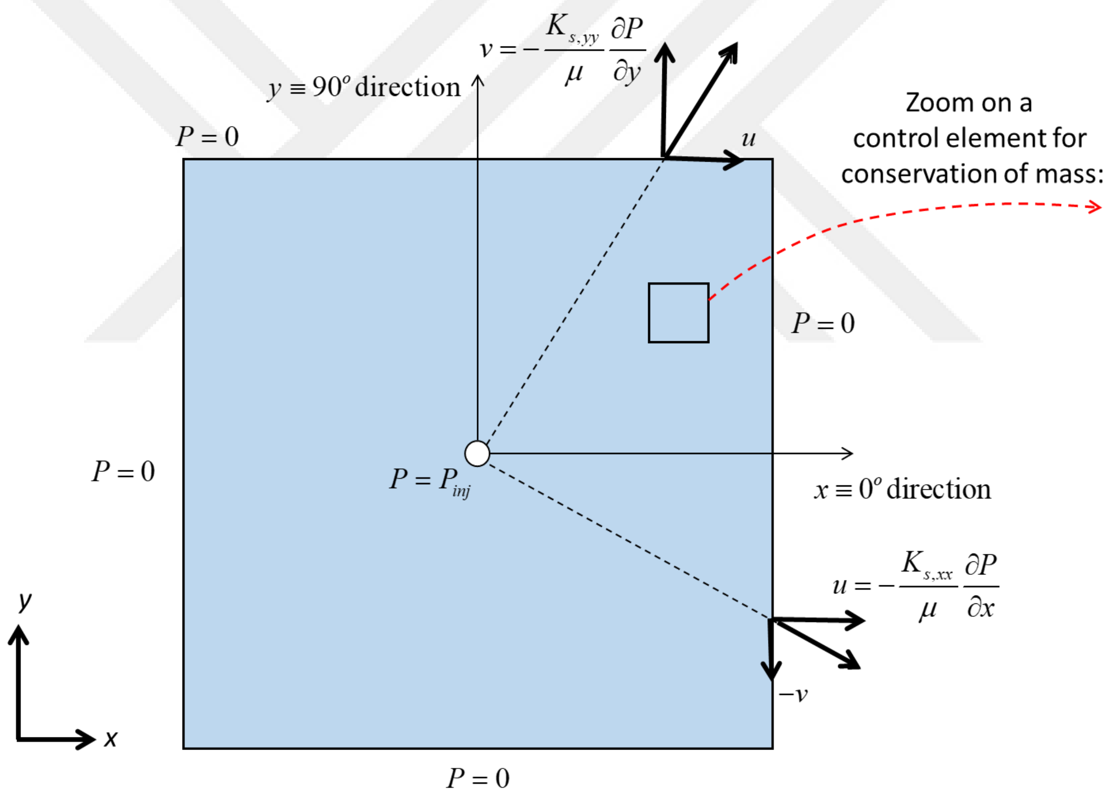

Figure 2.5 (a) The domain of the fabric specimen impregnated with resin at steady state 2D flow. Pressure boundary conditions at the inlet hole and around the outer periphery are shown.

The total outflow volumetric flow rate is calculated numerically as follows:

$$Q_{num} = \int_A U_n \circ \hat{n} \, dA \tag{2.10}$$

where A, U_n and $\hat{n}$ are the outer peripheral area of the fabric preform where the resin exits, normal outward velocity component and normal outward unit vector on A, respectively.

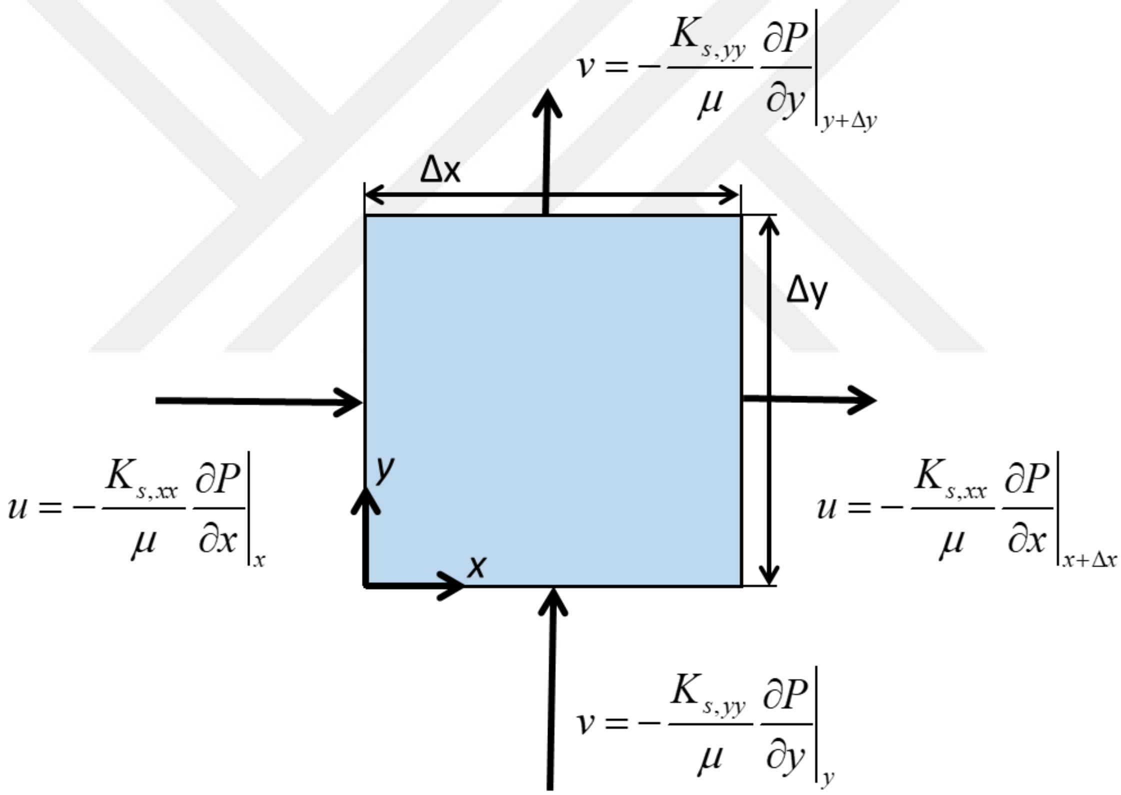

Figure 2.5 (b) The zoomed control element to derive the conservation of mass in the resin-filled domain.

2.3. Through-Thickness Permeability (K_z) Measurement Experiments under Constant-Injection Pressure Boundary Condition

During a through-thickness experiment, resin flow is created such that the resin enters from the bottom of the fabric preform and flows along the thickness direction (see Chapter 3 for detail). This experiment is performed only in steady flow regime.

The preform is fully impregnated with the resin, resin flushing from the exit (located at the top of the specimen) is continued for a while to reach steady state, and then the steady mass flow rate is measured.

Once the fluid reaches the outlet, the fluid is collected in a container whose mass, m, is recorded over time using a digital scale. The slope of the mass versus time, dm/dt, is determined. The volumetric flow rate Q is obtained by dividing the slope of dm/dt to the density of the resin ρ.

Steady through-thickness permeability, K_z of the fabric preform under constant-injection pressure boundary condition is calculated by using 1D Darcy's Law:

$$K_z = \frac{Q\,\mu\,h}{S\,\Delta P} \tag{2.11}$$

where μ is the viscosity of the resin, h is the thickness of the fabric preform, S is the cross-sectional area of the flow channel (which is equal to the top surface area of the fabric specimen) and ΔP is the pressure difference between the bottom and top surfaces of the fabric [10]. This pressure difference is computed as $\Delta P = P_{inj,gage} - \rho g \Delta L$ where ΔL is the vertical distance between the inlet resin pressure pot and the digital scale at the top (see Chapter 3 for detailed figure), and g is the gravitational acceleration.

Chapter 3
MATERIALS AND EXPERIMENTAL METHODS

3.1. Materials

Permeability characterization of a biaxial (0°/90°) E-glass fabric (Metyx LT850) was done at different fiber volume fractions by using silicone oil (Xiameter PMX 200) as a dummy resin (i.e., test fluid) in experiments. The top view of the fabric was shown in Fig. 3.1.b. Material properties such as fabric superficial density per layer and oil viscosity are given in Table 3.1.

Before each experiment, the temperature of the silicone oil is measured by using a sensor (Keller PAA 35 X). For the oil used, viscosity versus temperature characterization was earlier done and provided by Technical University of Munich (see Table 3.2 and Fig. 3.2) as a part of benchmark study among 10+ institutes. Arrhenius equation [11], $\mu = Ae^{-E_a/RT}$ was fit to the mentioned experimental data by using least squares method. The constants R, A, E_α were determined as 8.3144598 Joule/°K.mol, 2.8858 x10^{-4} Pa.s and $-$1.4376 x10^{-4} Joule/mol, respectively (see Fig. 3.2 for both the experimental data and the curve fit).

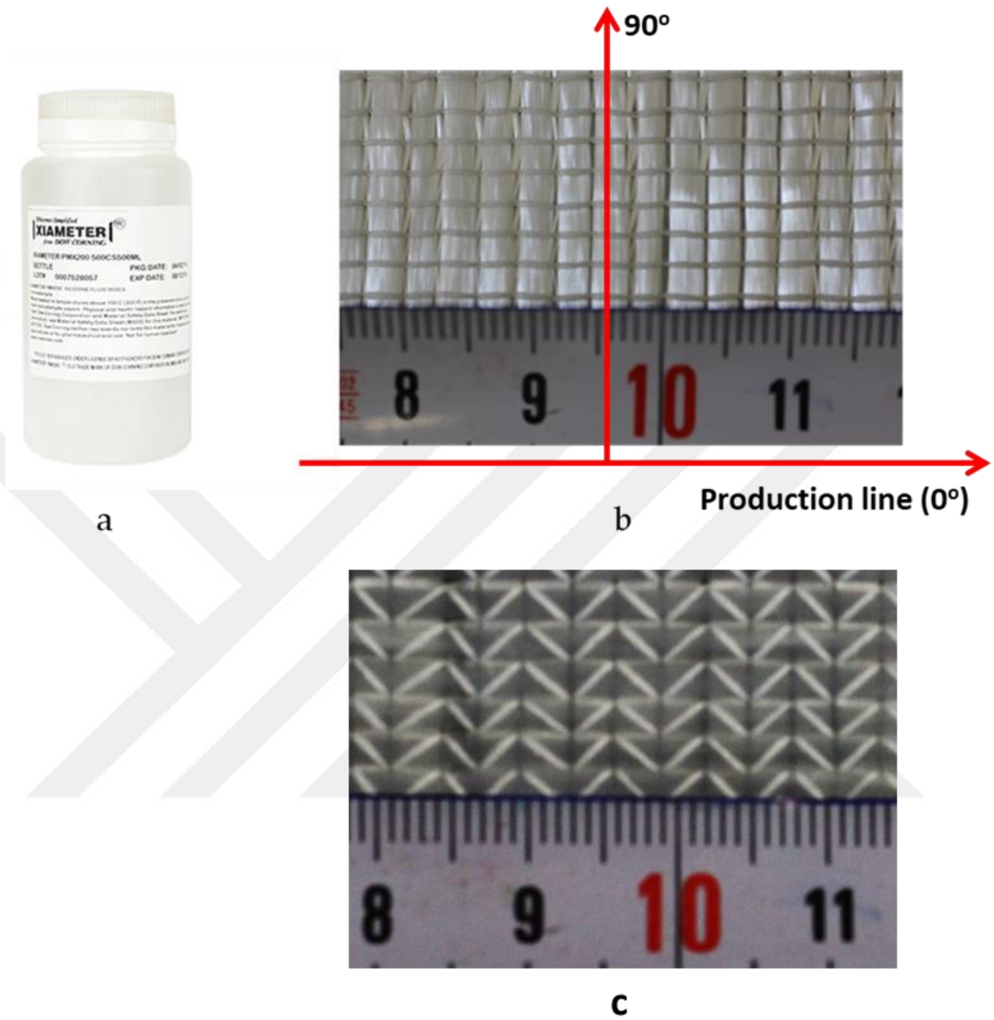

Figure 3.1 (a) Xiameter PMX 200 silicone oil, (b) top view and (c) bottom view of Metyc E-glass biaxial fabric.

Table 3.1. Material properties

Silicone Oil (test fluid)	Viscosity [Pa.s], μ	$\mu = Ae^{-E_a/RT}$ where R = 8.3144598 Joule/°K.mol, A = 2.8858 x10^{-4} Pa.s, E_α = −1.4376 x10^{-4} Joule/mol
Biaxial Fabric (0°/90°)	Superficial density per layer [g/m^2], ρ_{sup}	850
	Number of layers in the preform, n	5
	Bulk density of glass fibers [kg/m^3], ρ_{bulk}	2540
	Thickness (compacted) [m], h	0.003, 0.0035, 0.004
	Nominal fiber volume fraction, V_f (experimental values differed from the nominal values they were computed by measuring the mass and fiber volume fraction)	0.558, 0.478, 0.418

Table 3.2 Viscosity of the silicone oil versus temperature as characterized by Technical University of Munich (partially tabulated).

Temperature [°C]	Viscosity [mPa·s]	Temperature [°C]	Viscosity [mPa·s]	Temperature [°C]	Viscosity [mPa·s]
15.00	118.54	…	...	...	…
15.00	118.40	22.86	98.70	39.08	73.91
15.00	118.48	22.94	98.15	39.16	73.71
15.00	118.42	23.03	98.06	39.25	73.7
15.00	118.34	23.11	97.82	39.33	73.36
15.00	118.44	23.19	97.86	39.41	73.27
15.00	118.24	23.28	97.66	39.50	73.34
15.00	118.38	23.36	97.58	39.58	73.14
15.00	118.25	23.44	97.19	39.66	73.20
15.00	118.18	23.53	96.95	39.75	72.96
15.00	118.29	23.61	96.99	39.83	72.73
15.00	118.11	23.70	96.78	39.91	72.82
15.00	118.20	23.78	96.72	40.00	72.62
15.00	118.10	23.86	96.62	40.03	72.71
15.00	118.05	23.95	96.08	40.04	72.64
15.00	118.15	24.03	96.12	40.05	72.62
15.00	118.01	24.11	95.90	40.05	72.77
15.00	118.09	24.20	95.85	40.05	72.64
15.00	117.99	24.28	95.80	40.05	72.76
15.00	118.01	24.36	95.35	40.05	72.72
15.00	118.15	24.45	95.27	40.05	72.71
15.00	117.90	24.53	95.03	40.05	72.87
15.00	118.05	24.61	94.99	40.04	72.75
15.00	117.98	24.70	94.98	40.04	72.88
15.00	117.88	24.78	94.75	40.04	72.86
15.05	117.96	24.86	94.54	40.04	72.88
15.12	117.71	24.95	94.28	40.04	73.03
15.2	117.73	25.03	94.21	40.04	72.93
15.28	117.09	25.11	94.20	40.04	73.16
15.36	116.95	25.19	93.98	40.04	73.08
15.44	116.88	25.28	94.05	40.04	73.17
15.52	116.57	25.36	93.52	40.04	73.3
15.61	116.55	25.44	93.48	40.03	73.18
…	...	…	...	40.03	73.32

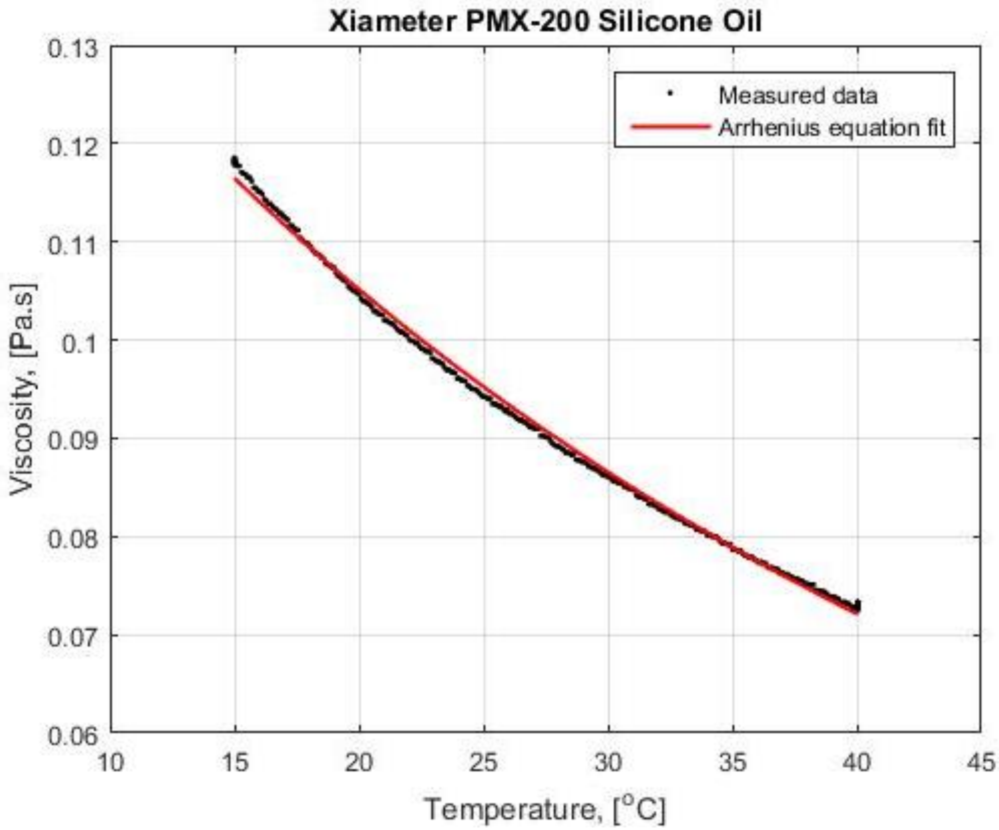

Figure 3.2 Viscosity of the silicone oil (Xiameter PMX 200) versus temperature as characterized by Technical University of Munich.

In addition, prior to an experiment, a viscosity measurement equipment is used to validate the viscosity of the resin calculated by Arrhenius equation. However, this is a rough validation as the precision of the equipment is low.

3.2. 1D Permeability Measurement Experimental Setup

1D permeability measurement experiments are conducted under constant pressure boundary conditions for both unsteady and steady flow regimes. The inlet reservoir is open to atmosphere and the exit is connected to a resin trap and a vacuum pump to create a predetermined level of vacuum pressure and thus a pressure differential of 80 kPa between the inlet and exit (see Fig. 3.3).

1D permeability measurement experiment at each of the three fiber volume fractions (corresponding to three different thickness values of 3.00, 3.50 and 4.00 mm) is conducted five times by using five specimens to investigate the repeatability. One set is conducted for the permeability along 0^{o} (production line) and another set is for 90^{o} (transverse direction) of the biaxial fabric preform.

Fabric layers are stacked one by one on the steel mold plate by aligning them in such a way that the production lines overlap (i.e., no angular shift). Two flow meshes are placed on the two ends of the flat steel mold and adjacent to the ends of the fabric preform such that they are underneath the inlet and exit tubes and a bit extending on the preform so that a linear inlet and exit are generated (see Fig. 3.3). A tacky tape around the periphery and a vacuum bag on the preform seal the mold cavity. When the inlet valve is at off-position, the vacuum pump is run to adjust the vacuum pressure to 80 kPa so that the fabric preform is compacted under 80 kPa.

The glass lid is placed on the vacuum bag. The dial gages and the bolt system are used (see Fig. 3.3) to ensure a uniform mold gap (and thus a uniform preform thickness, h).

After the valve is opened, the resin starts to propagate through the fabric. A digital video camera (Canon EOS 550D) records the flow front propagation until the fabric preform is wetted completely [12].

Any significant thickness change at the four corners of the mold is monitored by using the four dial gages, and if necessary, the bolt system is screwed to adjust the gap to the original value.

After the resin reaches the exit, infusion of the resin is maintained for 120 seconds to reach steady state [12]. In this period, a digital scale (with 0.1 g resolution) measures the mass of the infused resin.

For data acquisition (DAQ), HGX-1000 Multipurpose Weight Controller (frequency of 250 Hz) records the infused mass of the resin over time.

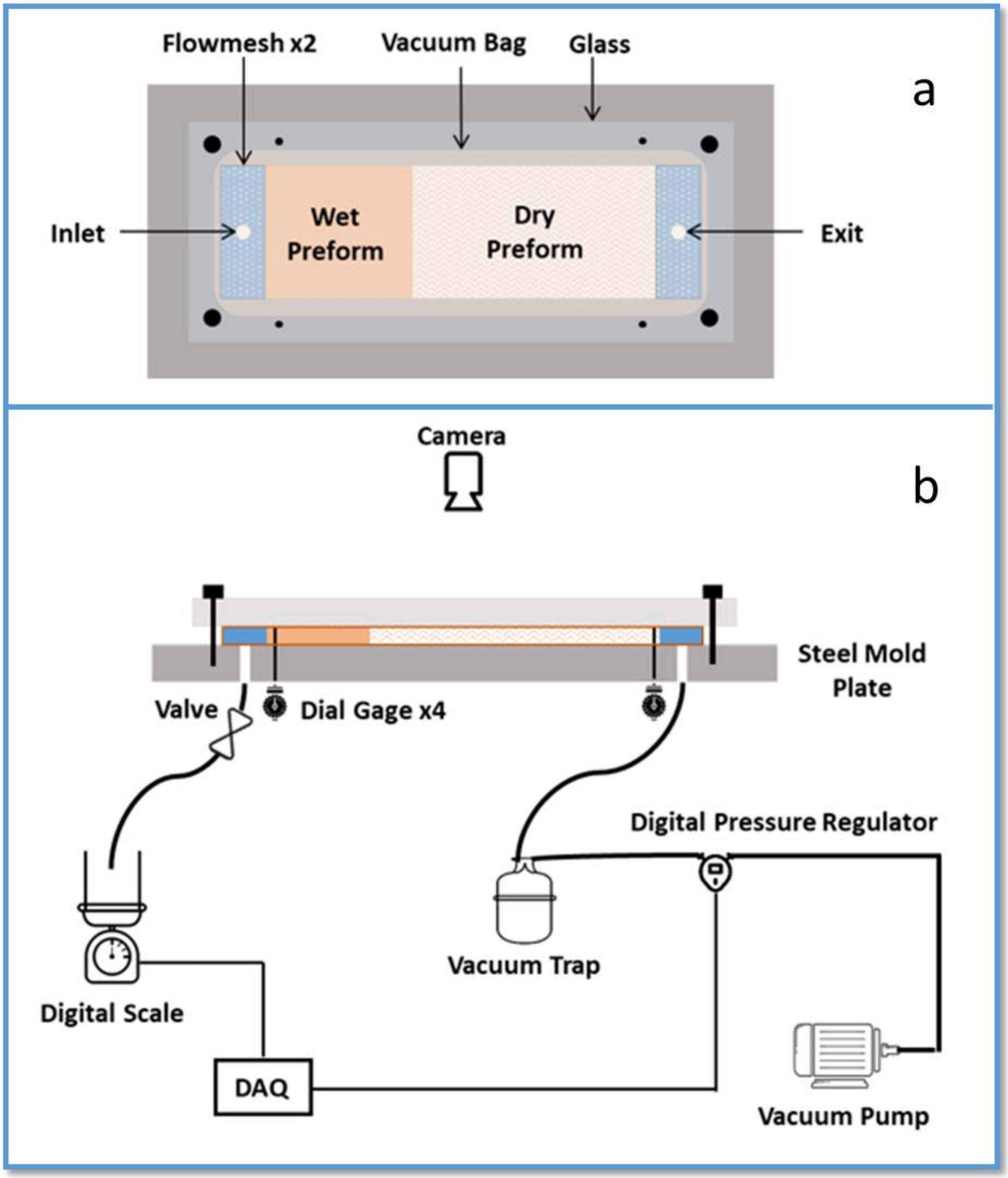

Figure 3.3 Schematic of 1D (linear) unsteady permeability measurement setup with an unsteady flow regime: (a) top view and (b) side view.

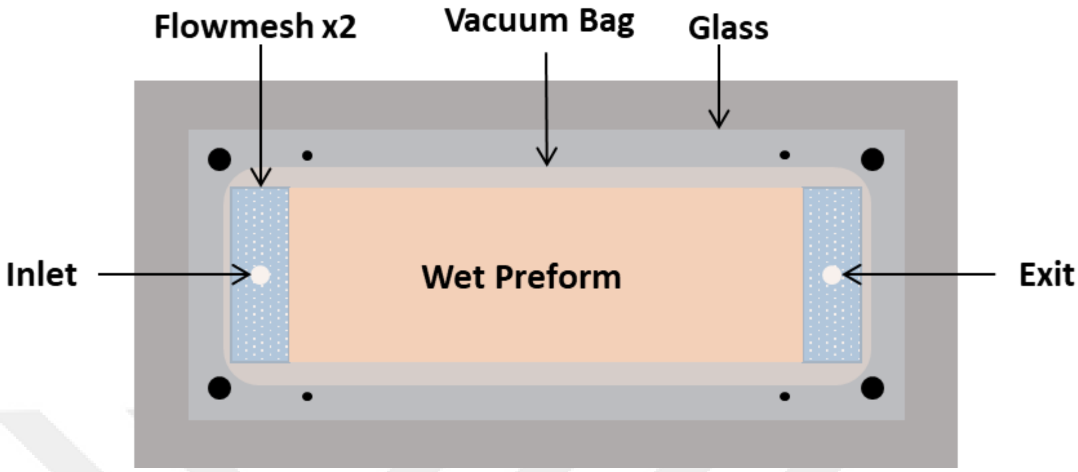

Figure 3.4 Top view of 1D (linear) steady permeability measurement setup with a steady flow regime.

3.3. 2D (Radial) Permeability Measurement Experimental Setup

Five layers of biaxial fabric are stacked and then punched (with a diameter of 12 mm) at their center. This fabric preform is placed on the lower mold plate made from aluminum (6000 series).

Eight steel spacers are placed on the lower mold to adjust the mold cavity thickness to either one of the three thicknesses of 3.0, 3.5 and 4.0 mm. Then, the aluminum (6000 series) upper mold plate with glass monitoring windows is compressed on the fabric specimen by using 16 latches and eight clamps (see Fig. 3.5 and 3.6).

The compressed air pressurizes the resin in the pressure pot to the desired injection value (80 kPa). An analog pressure regulator (CKD RP1000) is used to set this constant injection pressure value.

The resin pressure and temperature values are recorded by using a pressure and temperature sensor (Keller PAA 35 X, 0 to 10 bar abs, 0.002 full scale resolution). The viscosity of the resin is computed in Matlab by averaging the temperature values of the resin recorded during the experiment (no significant change in temperature occurs because a test fluid is used instead of an actual thermoset resin, and both the resin reservoir and the mold are at the same room temperature).

The resin flow through the mold cavity is initiated by setting the valve to open-position. Flow front propagation in through the glass inspection region (see Fig. 3.5 and 3.6) is recorded via a digital camera until the resin wets the fabric preform completely [12].

2D experimental setup has eight outlets along the edges of the lower mold plate so that the flushed resin is accumulated in the outlet digital scale (see Fig. 3.5 and 3.6) [12]. The mass versus time data of the resin is recorded via DAQ system.

After the resin comes out of the outlets, the resin flow is continued for 120 seconds (see Fig. 3.7.) to reach almost a steady state.

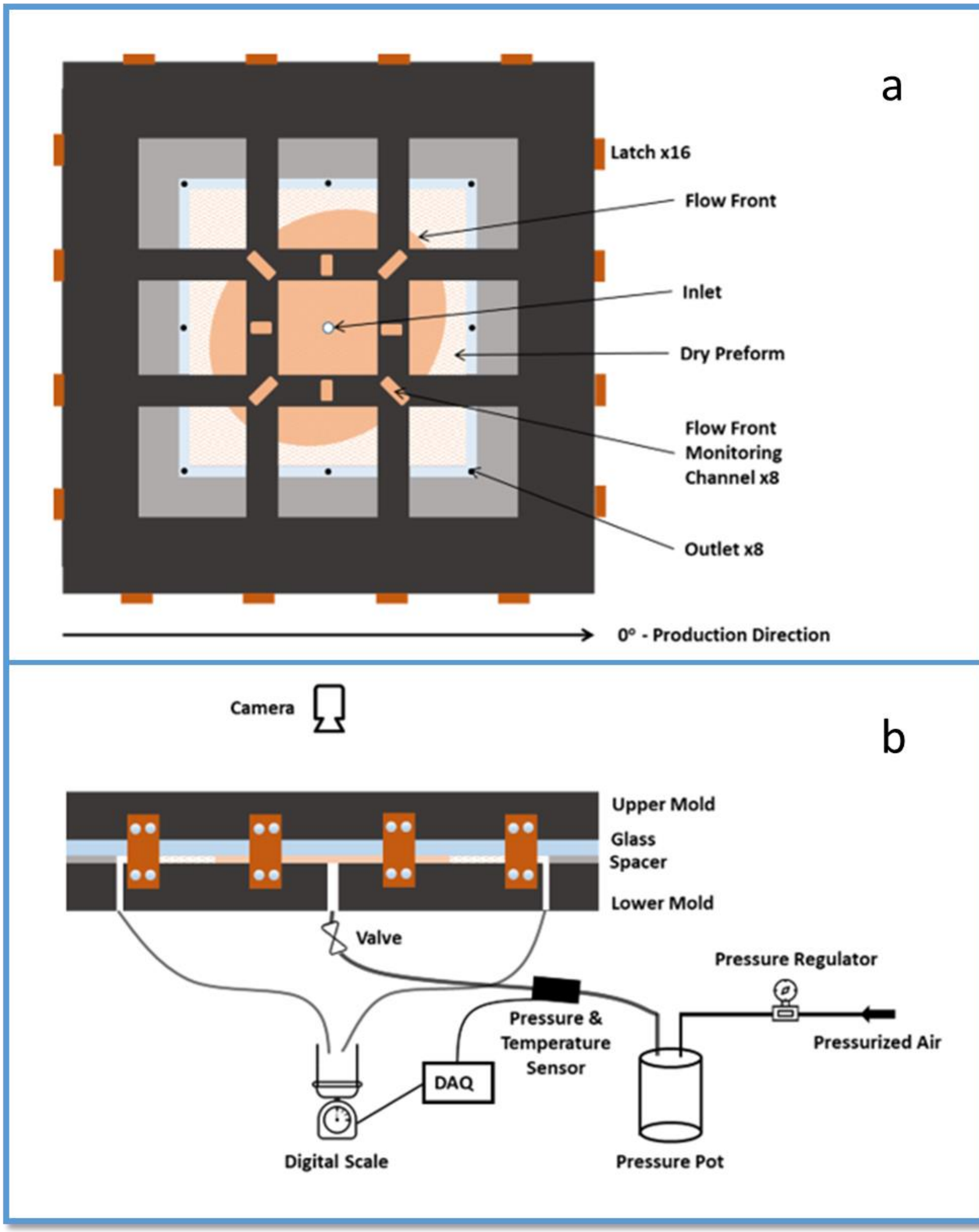

Figure 3.5 Schematic of 2D (radial) unsteady permeability measurement setup with an unsteady flow regime: (a) top view and (b) side view.

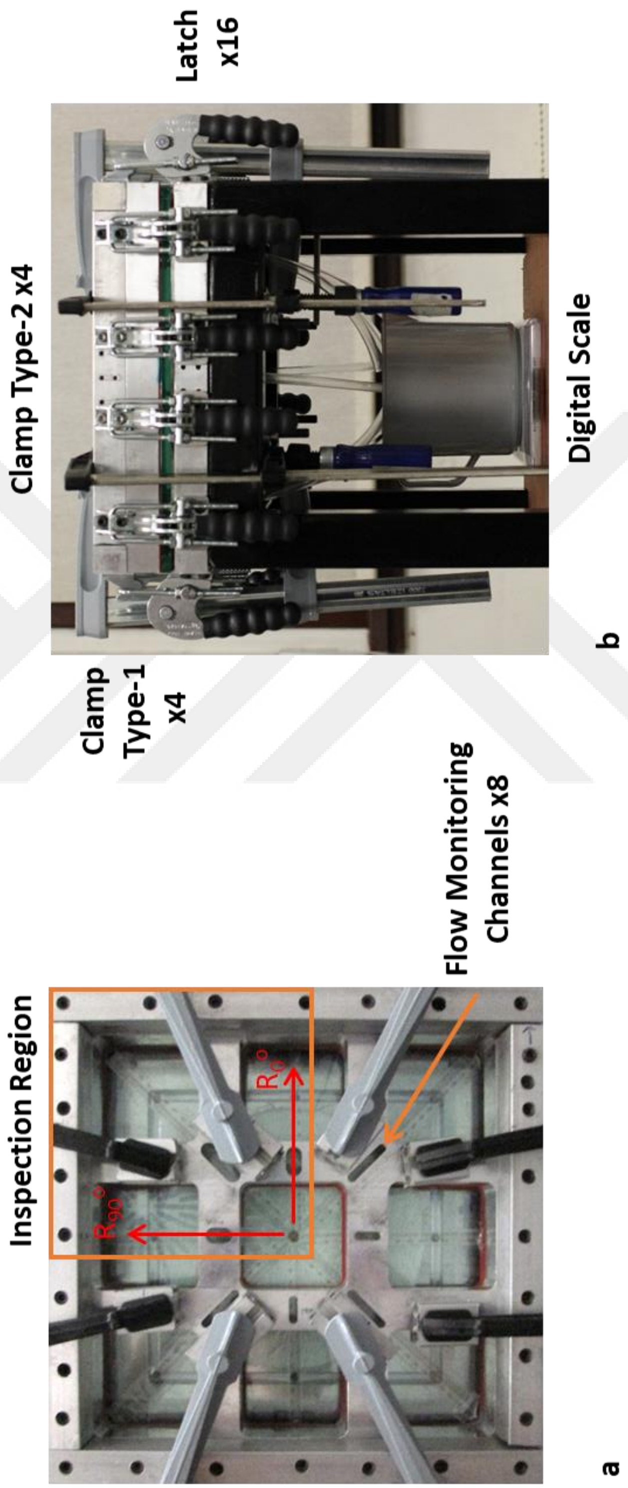

Figure 3.6 2D (radial) permeability measurement setup (a) top view and (b) side view.

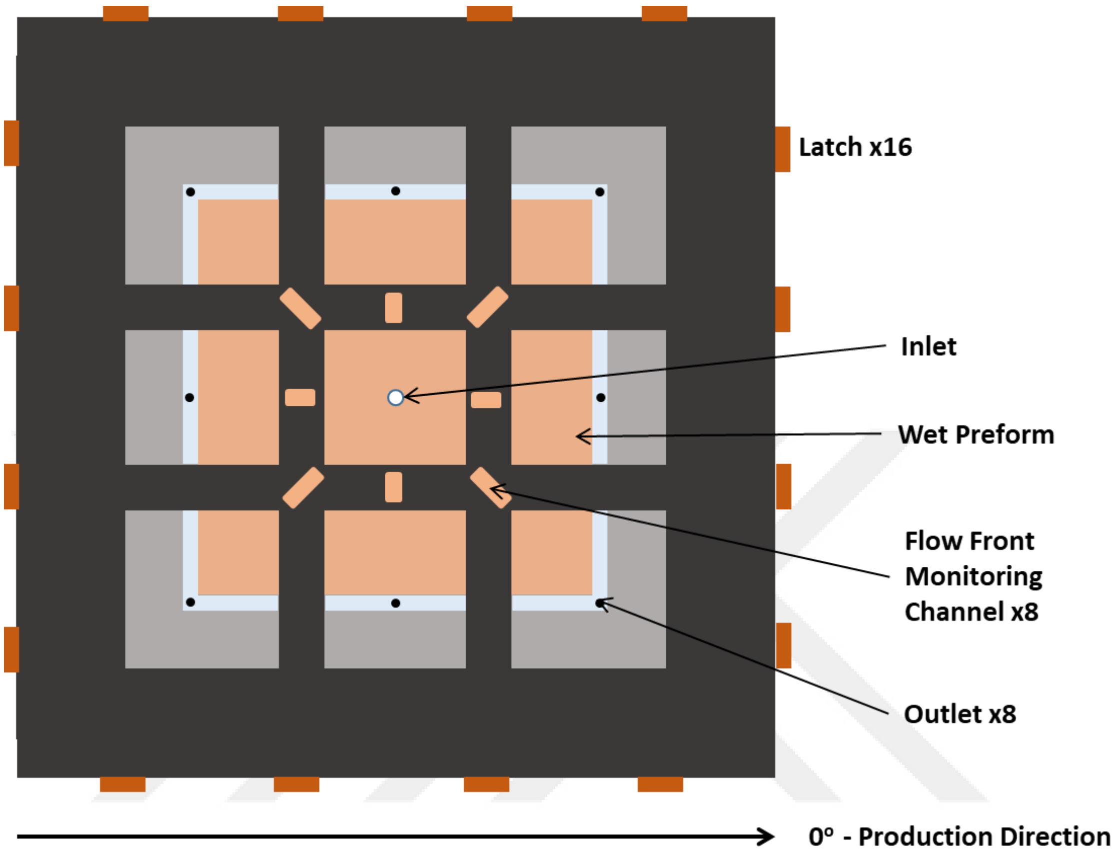

Figure 3.7 Top view of 2D (radial) permeability measurement setup with a steady flow regime (i.e., the fabric specimen is completely saturated, but the resin infusion is continued by keeping the inlet and exit open).

3.4. Through-Thickness Permeability Measurement Experimental Setup

The experimental setup is shown in Fig. 3.8. A stainless-steel flange (a thickness of 1 mm, an inner diameter of 95 mm, and an outer diameter of 98.2 mm) is glued to the aluminum (6000 series) lower mold half that is kept inside the aluminum (6000 series) tube.

A stainless-steel ring (with a thickness of 10.00 ± 0.03 mm) is placed on the lower mold. A circular fabric preform with a diameter of 95 mm is made by stacking ten plies and then it is placed into the metal ring.

Then, the second flange is fitted on the fabric preform concentrically and the aluminum (6000 series) upper mold is placed on the metal ring.

After the mold is compacted by using four bolts and eight nuts, the height between the lower and upper molds are checked whether it is 65.8 mm (see Fig. 3.8) to ensure that the mold is compacted properly (i.e., the fabric specimen is completely compacted in the ring). This setup fixes the mold cavity thickness and thus the thickness of the specimen to 10.00 ± 0.03 mm.

The disassembled components are shown in Fig. 3.9.

By using an analog pressure regulator, the resin injection pressure is fixed to 100 kPa. The valve is opened, and the resin injection is started.

After the resin arrives the exit, the injection is continued for 360 seconds to ensure that steady state flow rate is achieved. Only the mass data of the last 120 seconds is used in the flow rate calculation.

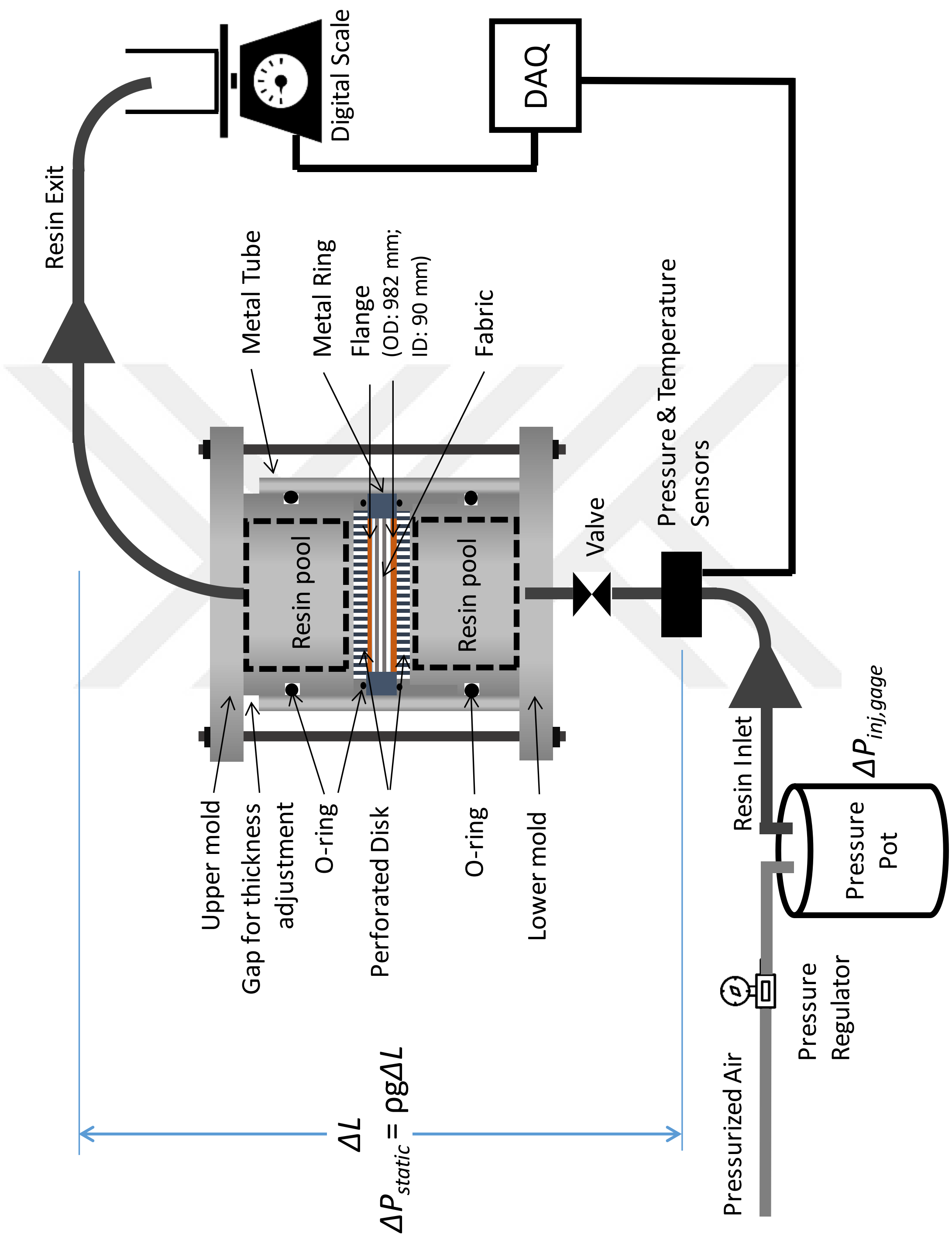

Figure 3.8 Schematic of the steady through-thickness permeability measurement setup with a steady flow regime.

a. Side view of the aluminum lower plate (inlet Ø12 mm).

b. Top view of the aluminum lower plate (200 mm x 200 mm x 30 mm).

c. Aluminum lower honeycomb (Ø138 mm).

d. Aluminum spacer (inner Ø98.2 mm - outer Ø138 mm).

e. Aluminum tube (inner Ø138 mm - outer Ø158 mm).

f. Stainless steel lower flange (inner Ø90 mm - outer Ø98.2 mm).

Figure 3.9 (a-f) Disassembled components of the through-thickness permeability measurement setup.

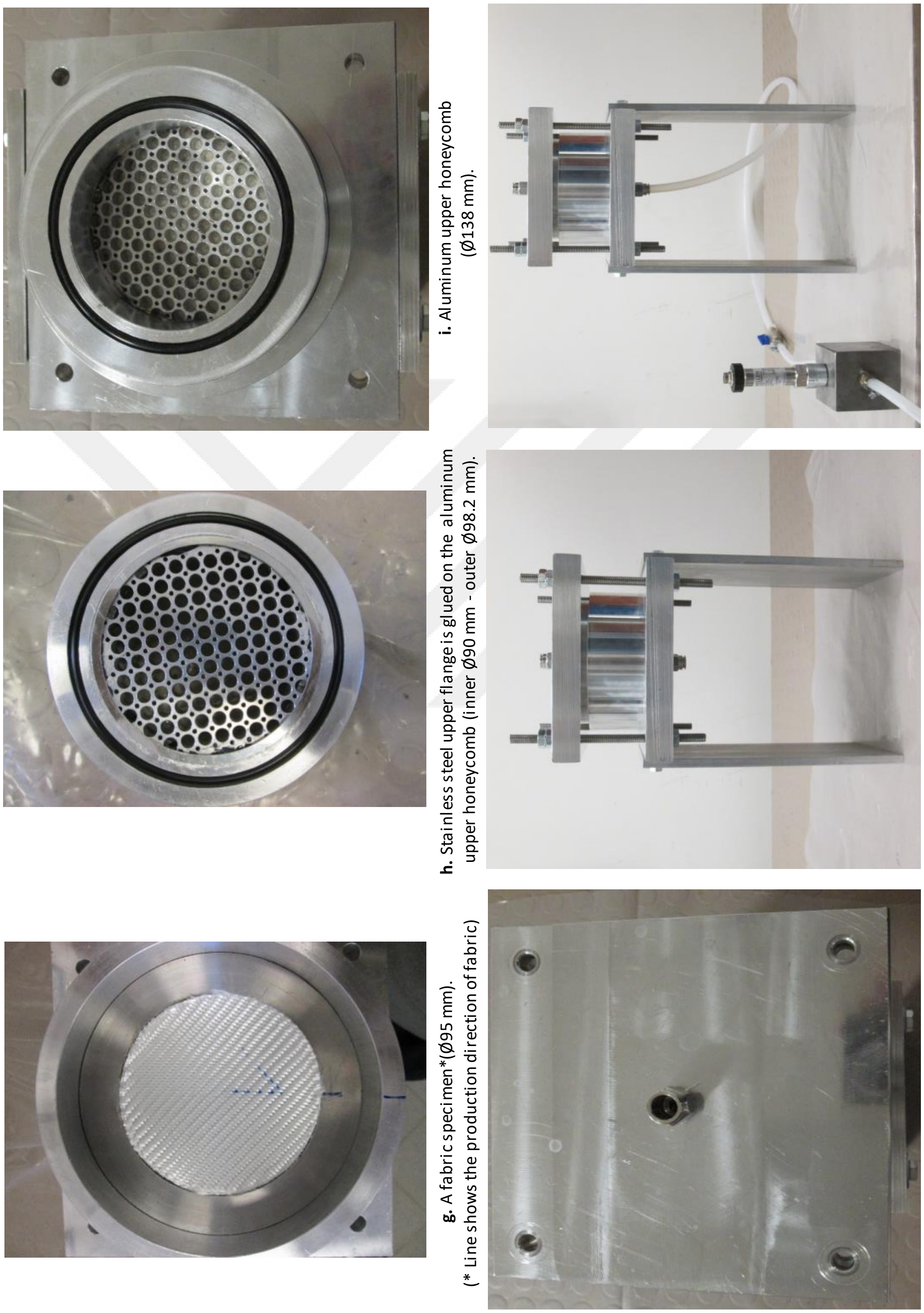

Figure 3.9 (g-l) Disassembled components of the through-thickness permeability measurement setup.

Fig.14. Galvanize pressure pot
(Max. working pressure: 4.5 bar)

Fig.13. Placement of corn syrup inside the pressure pot

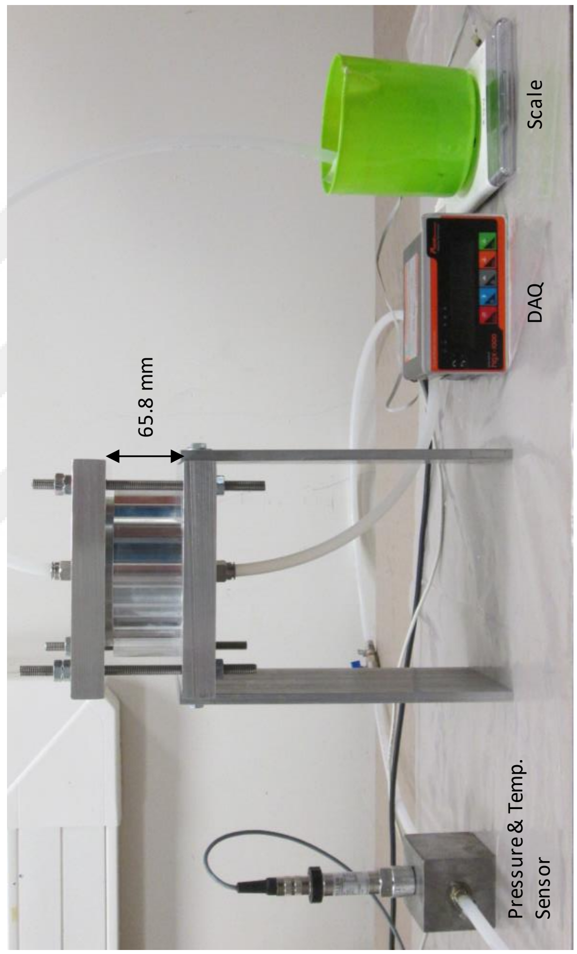

Fig.15. Through Thickness Permeability Characterization Setup
(Resolution of scale: 0.1 g)

Figure 3.9 (m-o) Disassembled components of the through-thickness permeability measurement setup.

Chapter 4
PROCESSING EXPERIMENTAL DATA TO DETERMINE PERMEABILITY

In this chapter, four common curve fitting methods in the literature will be reviewed. These are (1) global method, (2) single-step method, (3) reference time step method, and (4) elementary method. In general, they all use least squares method by fitting a best curve fit to all or some of the experimental data. The details are briefly given later in this chapter.

Depending on what permeability characterization (1D or radial; unsteady or steady), propagation of flow front position with time, $x_f(t)$ or $r_f(t)$ were derived in the literature and reviewed earlier in this study. They are either in closed form or in an equation that the flow front term could not be left alone (see Chapter 2). In this chapter, the curve fitting methods will be applied to fit either (1) the analytical closed-form flow front position equation which has process parameters (fiber volume fraction, pressure differential between the inlet and exit, resin viscosity, mold dimensions and preform permeability), or (2) a form of the expression that involves the flow front position.

The analytical expression for the flow front position of resin, $x_f(t)$ during 1D (linear) unsteady experiment is given below (see Chapter 2):

$$x_f = \sqrt{\frac{2K\Delta P\, t}{\mu\phi}} \equiv \sqrt{C\, t} \tag{4.1}$$

The numerical curve fit formula will include an additional constant, B to overcome the experimental error induced by inaccurate setting of the initial time:

$$x_f = \mathrm{A}\sqrt{t} + \mathrm{B} \tag{4.2}$$

That means, $A = \sqrt{C}$ where C appears in Eq. 4.1. The constants A and B are determined by curve fitting Eq. 4.2 to the experimental data by using least squares method. The curve fitting is done to either the complete data set or partially (and taking the average of the permeability values whenever multiple values are computed) in the aforementioned four methods.

After computing C, it is substituted (along with other parameters used in the characterization experiment) into the formula below to calculate the unsteady permeability K_{uns}

$$K_{uns} = \frac{C\, \mu\, \phi}{2\, \Delta P} \tag{4.3}$$

Only global method is applied to calculate 1D saturated permeability.

For 2D (radial) unsaturated experiments, K_{uns} can be left alone on the left hand side of the following analytical equation (see Chapter 2):

$$K_{uns} = \frac{\mu\, \phi}{4P_{in}} \left\{ r_f^2 \left(2\, ln\left(\frac{r_f}{r_0}\right) - 1 \right) + r_0^2 \right\} \frac{1}{t} \tag{4.4}$$

Eq. 4.4 looks a bit confusing due to the fact that the left hand side is K_{uns} which is constant (i.e., does not vary with time), however the right hand side is a function of time as it includes $r_f(t)$ and t. A careful analysis results in that the right hand side does not vary with time because it must also be a constant. However, due to the experimental errors involved, it is practically never constant, but varying slightly over time. To handle this and have a standard way of computing K_{uns}, Eq. 4.4 is rewritten as follows:

$$F(t) \equiv K_{uns}\, t = \frac{\mu\, \phi}{4P_{in}} \left\{ r_f^2 \left(2\, ln \left(\frac{r_f}{r_0} \right) - 1 \right) + r_0^2 \right\} \qquad (4.5)$$

Now, $F(t)$ is expected to be a linear function of time, t. We are interested in calculating K_{uns}. The right hand side of Eq. 4.5 versus time will be plotted, and the slope of the curve is assigned as K_{uns}. All of the four curve fitting methods will be used separately for this 2D unsteady flow case.

Permeability for 2D steady flow case will be computed as described in Chapter 2 by matching the numerically computed outflow rate to the experimental outflow rate. This approach uses the ratios of the unsteady and steady permeability components along the two orthogonal directions (production lineand transverse direction) the same, but iterates their values in the numerical solution while checking if matching is achieved.

4.1. Global Method

This method is the most common method applied. It fits the analytically expected formula (see above and also Chapter 2 for details) to ***all*** experimental data [13] as schematically described in Fig. 4.1.

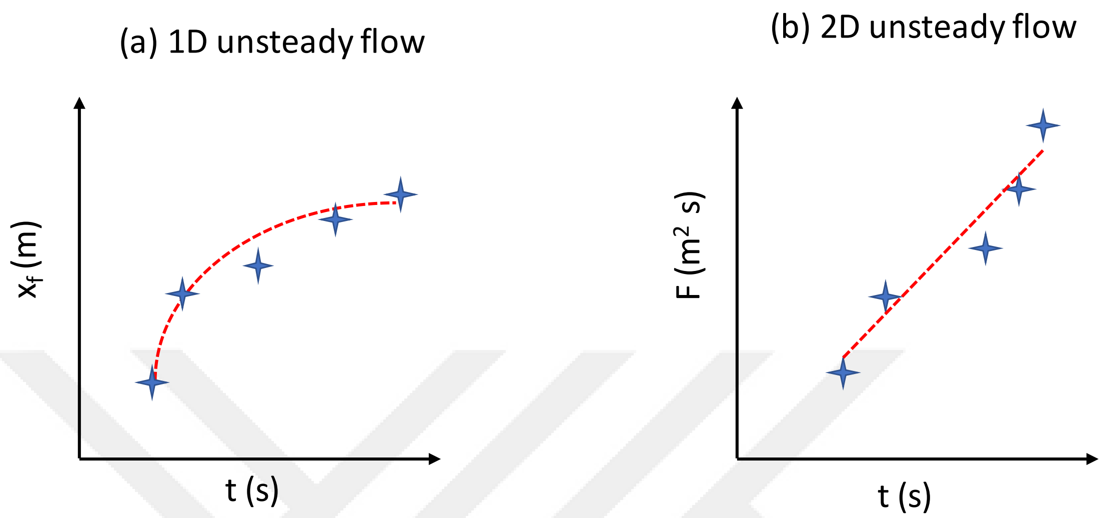

Figure 4.1 Schematic of global method which fits one best curve fit (red line) to the full set of experimental data.

4.2. Single-Step Method

This method fits the analytically expected formula to only ***two*** experimental data (the filled blue stars shown in Fig. 4.2), but not to all [13]. The data around the mid region of the mold is taken due to two major reasons: (1) the initial data may include more error in it due to fast resin flow, and (2) the last part may deviate from the expected flow (linear flow front in 1D, and perfect elliptical front in radial flow).

For 1D unsaturated flow experiment, resin arrival data at $x_f = 0.100$ and 0.200 m were used. For 2D unsaturated flow experiment, resin arrival data approximately at $r_{f,0} = 0.050$ and 0.080 m, and $r_{f,90} = 0.040$ and 0.060 m are used.

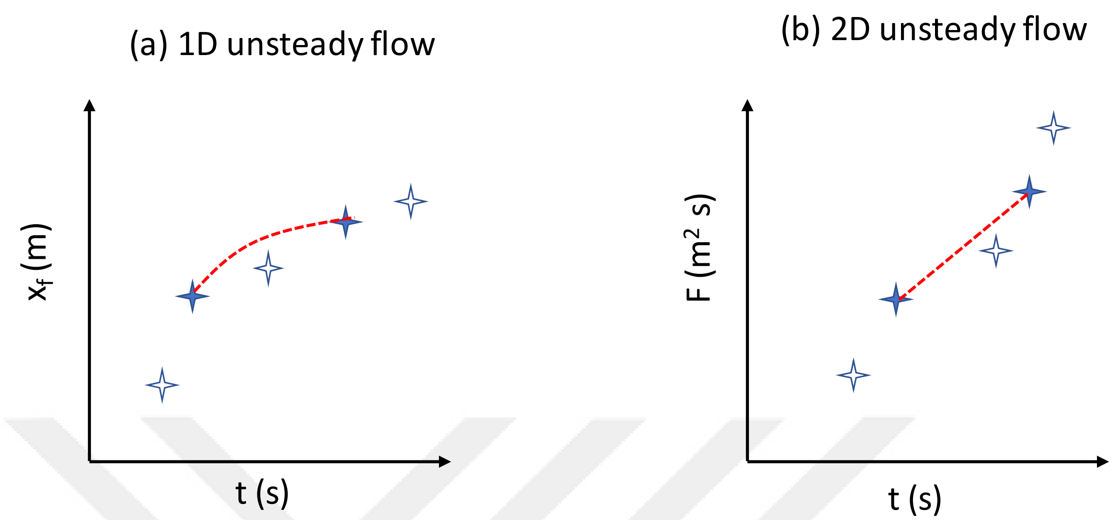

Figure 4.2 Schematic of single-step method which fits the analytically expected formula to only ***two*** experimental data (the filled blue stars), but not to all data.

4.3. Reference Time Step Method

This method fits the analytically expected formula to ***a set of two experimental data*** (i.e., 1st and 2nd, 1st and 3rd, 1st and 4th, …, 1st and Nth as shown in Fig. 4.3) such that the first data is always used. The results calculated are then averaged.

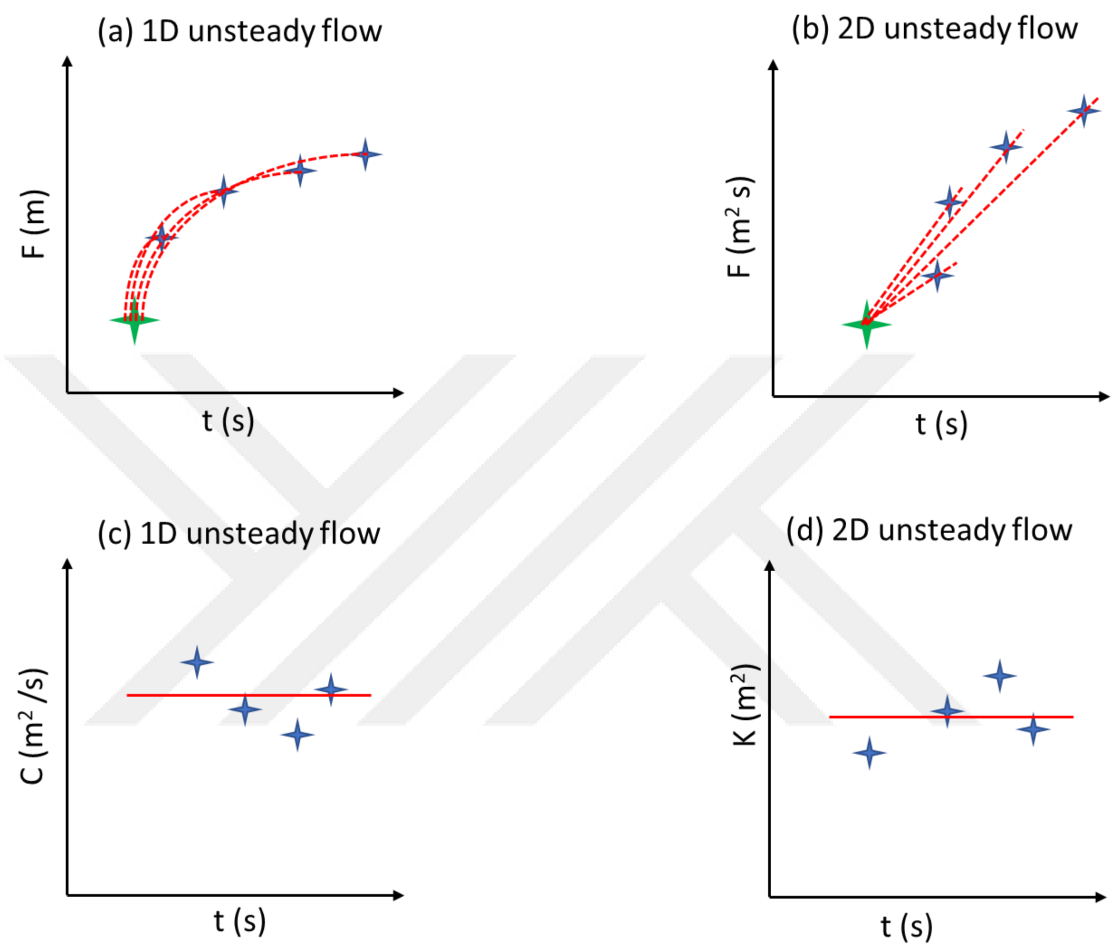

Figure 4.4 (a) and (b): Schematic of reference time step method which fits the analytically expected formula to 1st and 2nd, 1st and 3rd, 1st and 4th, …, 1st and Nth data separately.

(c) and (d): N-1 results calculated in (a) and (b) are averaged.

4.4. Elementary Method

This method fits the analytically expected formula to a set of data pairs (1st and 2nd, 2nd and 3rd, 3rd and 4th, …, (N-1)th and Nth) separately [13] as shown in Fig. 4.4. The results calculated are then averaged.

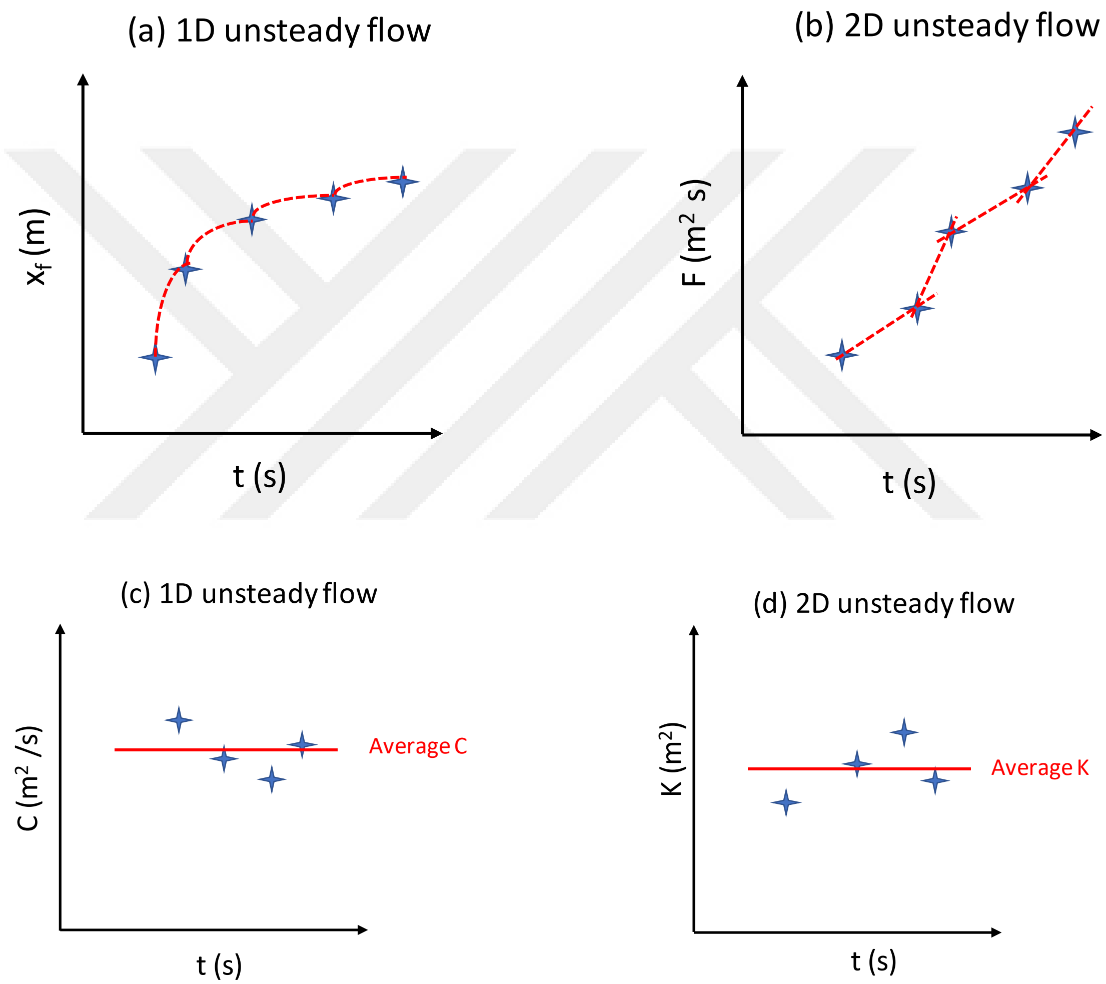

Fig. 4.3. (a) and (b): Schematic of elementary method which fits the analytically expected formula to 1st and 2nd, 2nd and 3rd, 3rd and 4th, …, (N-1)th and Nth data separately.

(c) and (d): N-1 results calculated in (a) and (b) are averaged.

4.5. R-squared measure

In this study, it will be investigated how closely aforementioned four curve fitting methods fit to the experimental data by comparing their *R-squared* values.

R-squared (R^2) is a measure of "goodness of fit" in [0,1] interval [14]. $R^2 = 0$ means that it is the worst fit, and $R^2 = 1$ means that it is the best fit that passes through all data points. There is a relationship between *R-squared* value and the perfectness of the regression model [14].

R-squared is calculated by using the following formula [15]:

$$R^2 = \frac{SSY - SSE}{SSY} \tag{4.6}$$

where SSE and SSY are *the sum of squared errors of the model from corresponding data set* and *the sum of squared errors of the model from the average of the model values*, respectively.

For example, for a representative curve fit function of $y = a + bx$, SSE and SSY are calculated as follows

$$SSE = \sum (y - a - bx)^2 \tag{4.7}$$

$$SSY = \sum (y - \bar{y})^2 \tag{4.8}$$

where $\bar{y}$ is the average of y [15].

Chapter 5
RESULTS OF THE PREMEABILITY MEASUREMENT EXPERIMENTS

5.1. Permeability Results

In this chapter, the results of the permeability experiments conducted for 1D (linear) flow, 2D (radial) flow and through-thickness flow are examined. Due to a confidentiality agreement regarding the fabric material used in the through-thickness permeability measurements, only a sample through-thickness permeability result is presented without giving the specific details.

Four different evaluation methods introduced in Chapter 4 are used for the calculation of 1D and 2D unsteady permeabilities. The steady permeability calculation in 1D needs mass flow rate data which is obtained by using the *global method* only (i.e., by using a curve fit to the full data). The steady permeability calculation in 2D is computed by iterating the scale constant a in $K_{s,0}/K_{s,0} = a\,K_{uns,0}/K_{uns,0}$ while matching the numerical flow rate of the flow model in the mold cavity to the experimental flow rate (explained earlier in Chapter 4).

Results of 1D and 2D permeability measurements are presented in Fig. 5.1-5.14 along with the following exponential fits to the experimental data by using least squares as earlier used in the literature by Yalçınkaya et al. [4] and many other researchers

$$K = Ae^{-BV_f} \tag{5.1}$$

which can be rewritten as follows to have a first order relationsgip with new variables

$$\ln(K) = \ln(A) - BV_f \tag{5.2}$$

The following Matlab code is used for fitting to K versus V_f experimental data

```
% Take natural logarithm of both sides of Eq. 5.1:
%     ln(K) = ln(A)-B*Vf    Eq. 5.2
% Rename:
%     KK = ln(K)
%     D = -B
%     C = ln(A)
%     KK = D*Vf+C;
P = polyfit(Vf,log(K),1);
D = P(1);
C = P(2);
A = exp(C)
B = -D
Vffit = linspace(Vf(1),Vf(end),100);
Kfit = A*exp(-B*Vffit);
```

As mentioned in Chapter 4, *R-squared* (R^2) is used to compare the *goodness-of-fit* of the four curve-fitting methods. R^2 value is the highest for Global method in both 1D and 2D unsteady permeability results as presented in Tables 5.1 – 5.4. Although single step method is a simpler method since only two data points are used for the calculation, it can still provide good permeability results [13] as long as the data points are selected carefully as done in this study by using the data taken from the mid region of the mold. In addition, it is observed that the methods have higher R^2 value for 1D unsteady permeability measurements of

90° of the fabric preform because time interval between two subsequent data points is longer than corresponding value in 0° direction. Besides, the methods fit better to 1D experimental data than 2D experimental data as it can be figured out from R^2 values in Tables 5.1 – 5.4 that may arise from the data points that deviated from others very significantly. This also shows that significant variation in the composite material manufacturing can be observed by analyzing the scattered data mostly induced by nonuniform fabric structure and nonrepeatable fabric preparation labor (cutting, stacking and placement).

It can be easily observed from Fig. 5.1 -5.4 that the unsteady permeability of the fabric preform decreases with increasing fiber volume fraction for both 1D and 2D flow experiments, as expected. Also, elementary method provides highest permeability change with changing fiber volume fractions for 2D flow experiments. Single step method has large scatter for some of the experiment types.

In general, the variation among the repeated experiments (scatter) is smaller for 1D unsteady measurements than that of 2D measurements, the variation is less than 20%.

A quick comparison of the results obtained for 1D and 2D measurements, as presented in Fig. 5.5 and 5.6 and also in Table 5.1-5.4, 2D unsteady permeabilities are higher than 1D unsteady permeabilities, except for the highest fiber volume fraction. Additionally, the change in permeability by increasing fiber volume fraction is more prominent in 2D measurements.

It should be noted that the 2D permeability setup consists of metal on the bottom half and metal-supported glass on the top half, whereas 1D permeability setup consists of a glass top half and a metal bottom half. It is suspected that significant difference in the permeability trends may be partially due to load bearing capacities of the two setups resulting of deflections to different extents. 1D permeability setup is less stiff due to glass upper half and it is likely to be deflected more significantly especially at high fiber volume fractions and resulting in higher cavity thickness than expected which in turn increases the calculated permeability. However, even with very rigid mold materials and experienced staff, very significant variation among the repeated experiments and deviation between unsteady and steady permeabilities are very common in the literature [6]. Therefore, our explanation based on two different levels of deflection may not be the only reason of this aforementioned permeability difference.

1D and 2D steady permeability measurements are presented in Fig. 5.7-5.10 for both principal directions. 2D measurements show an expected trend where the permeability decreases by increasing fiber volume fraction, whereas 1D permeability results show an inverse trend, which is definitely unexpected. Fig. 5.11-5.12 present the results of the two measurement types together and highlights the deviation of the results with increasing fiber volume fraction.

In Fig. 5.13-5.14, 2D permeability measurement results are shown for both unsteady and steady flow regimes of two directions.

As pointed out above, 1D permeability setup is suspected to be subject to significant deflection, especially at higher fiber volume fractions. Cavity height is adjusted by using four dial gages located at the edges. However, the current configuration of the setup does not allow to measure the cavity height at the center of the mold where the deviation is expected to be the highest. The fabric thickness (i.e., the cavity height) is a divisor in the K_s equation (see Eq. 2.3) and substituting a higher thickness value in that equation would yield a lower permeability. However, the measurement of thickness at the center of the mold is not performed at this stage and will be included later, along with a bolt system included to the mid-section of the mold to adjust the thickness to the desired value.

Generally, the mean of the unsteady permeability results obtained from the four methods are close to each other, as expected because the four different methods have similar R^2 values. However, the standard deviations are high in some methods (such as single step method).

It should also be noted that the steady permeability results have larger scatter than the unsteady permeability results for both 1D and 2D experiments.

The sample calculations of 1D, 2D and through-thickness permeability experiments are presented at the end of this chapter.

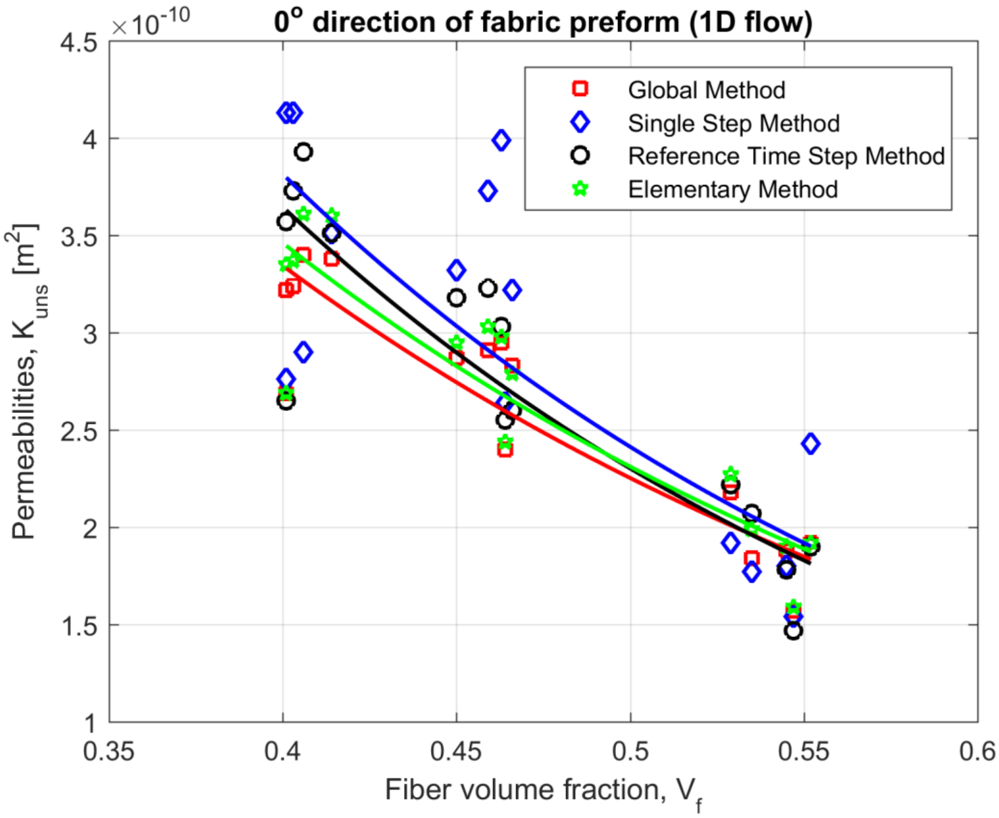

Figure 5.1 Results of 1D unsteady permeability experiments for 0° direction of fabric preform. Four different curve-fitting methods are applied to each raw experimental data to determine the permeability data (shown with symbols) at a fiber volume fraction. The solid lines are exponential fits (as detailed in Eq. 5.1) to all 15 (3*5) data.

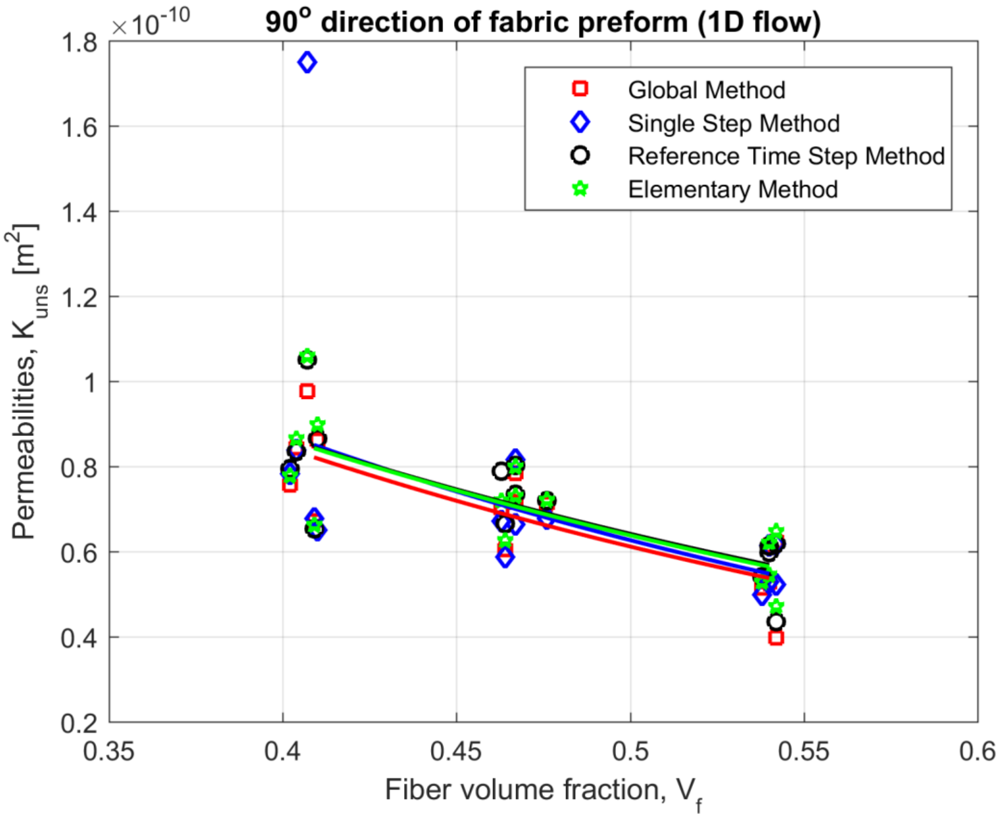

Figure 5.2 Results of 1D unsteady permeability experiments for 90° direction of fabric preform. Four different curve-fitting methods are applied to each raw experimental data to determine the permeability data (shown with symbols) at a fiber volume fraction. The solid lines are exponential fits (as detailed in Eq. 5.1) to all 15 (3*5) data.

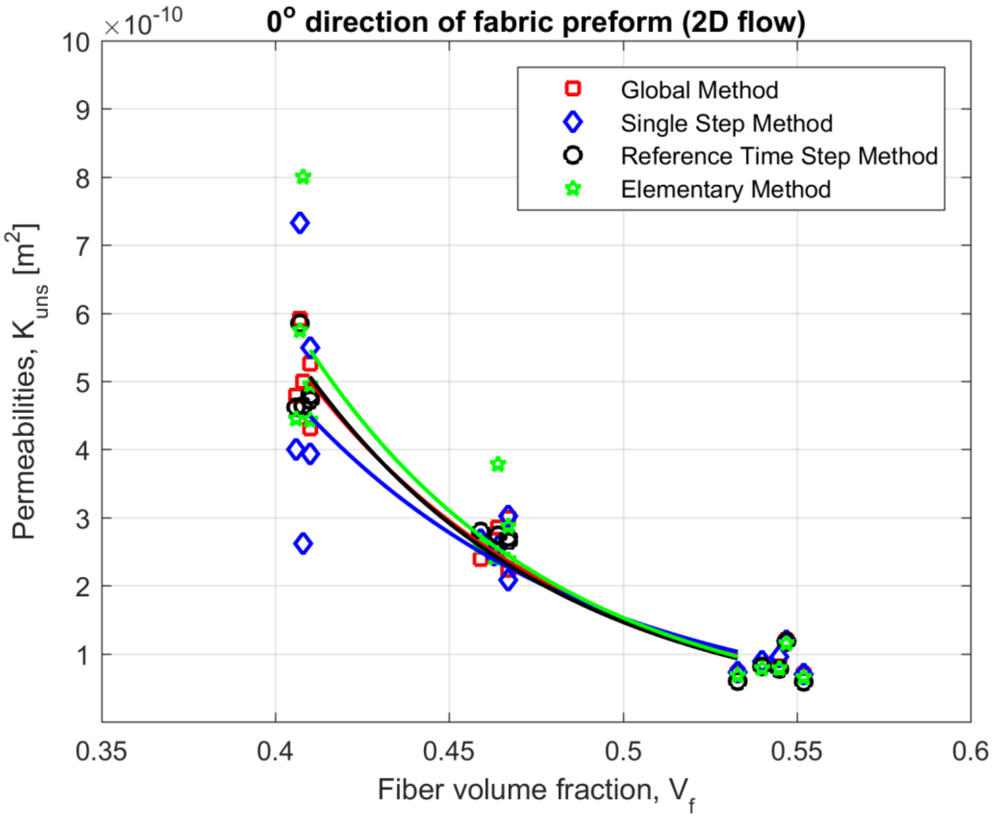

Figure 5.3 Results of 2D unsteady permeability experiments for 0° direction of fabric preform. Four different curve-fitting methods are applied to each raw experimental data to determine the permeability data (shown with symbols) at a fiber volume fraction. The solid lines are exponential fits (as detailed in Eq. 5.1) to all 15 (3*5) data.

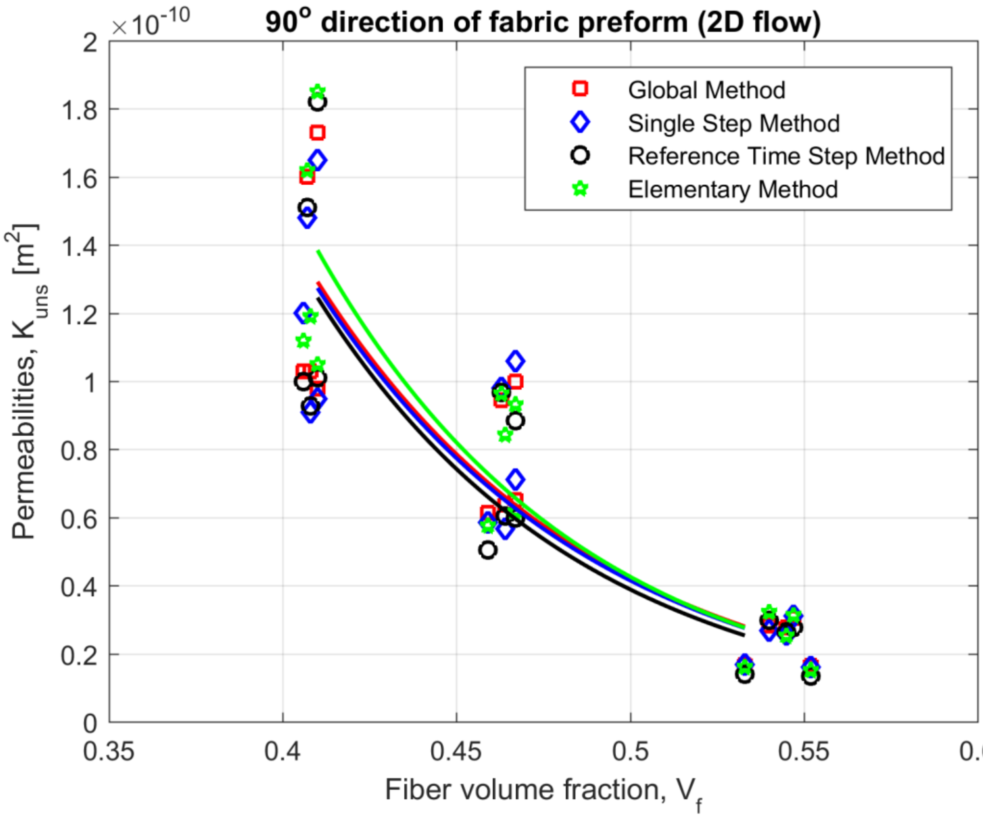

Figure 5.4 Results of 2D unsteady permeability experiments for 90° direction of fabric preform. Four different curve-fitting methods are applied to each raw experimental data to determine the permeability data (shown with symbols) at a fiber volume fraction. The solid lines are exponential fits (as detailed in Eq. 5.1) to all 15 (3*5) data.

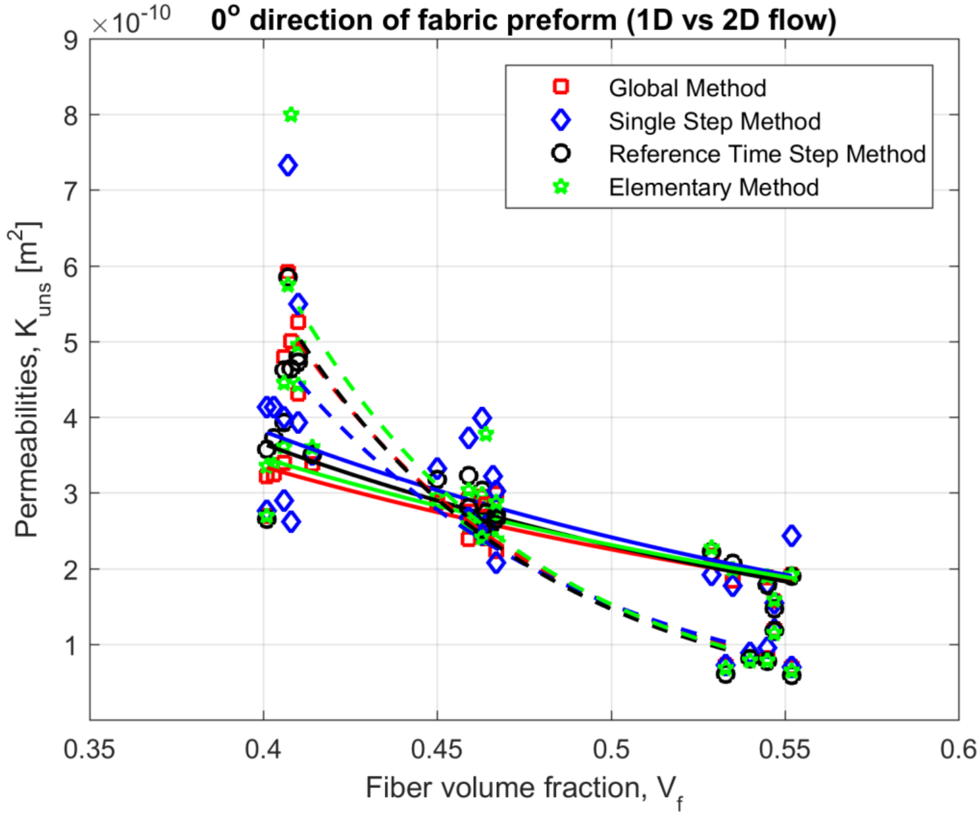

Figure 5.5 Results of 1D and 2D unsteady permeability experiments for 0° direction of fabric preform (solid lines: 1D permeability, dashed lines: 2D permeability).

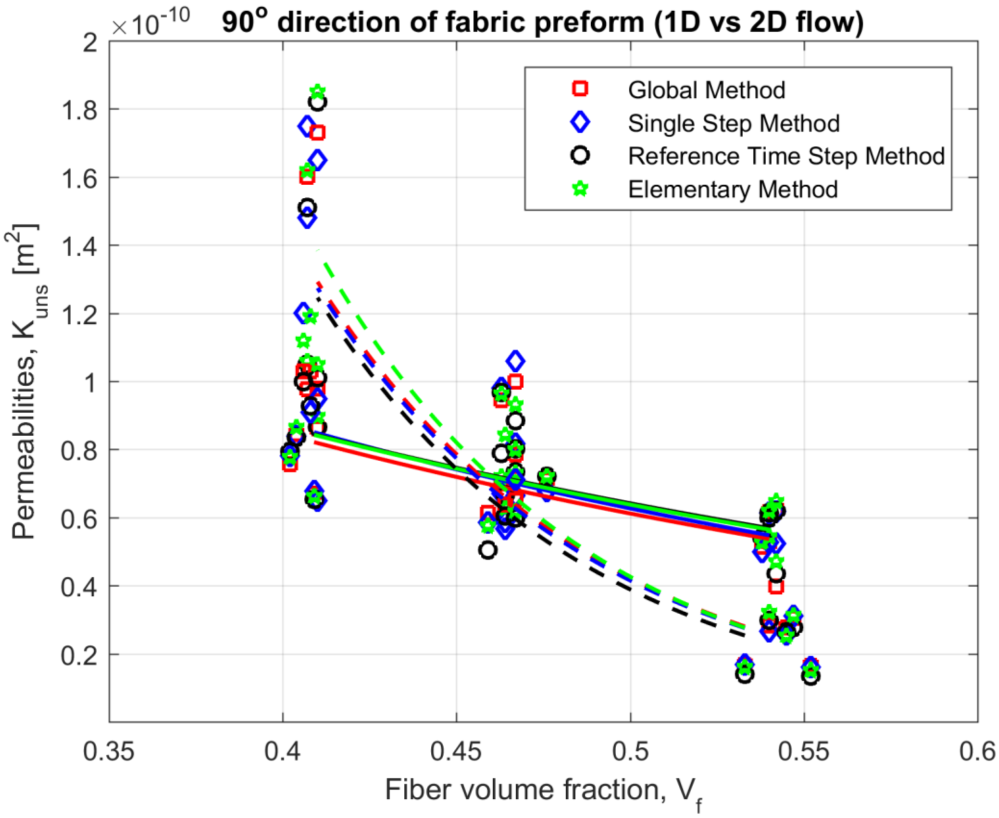

Figure 5.6 Results of 1D and 2D unsteady permeability experiments for 90° direction of fabric preform (solid lines: 1D permeability, dashed lines: 2D permeability).

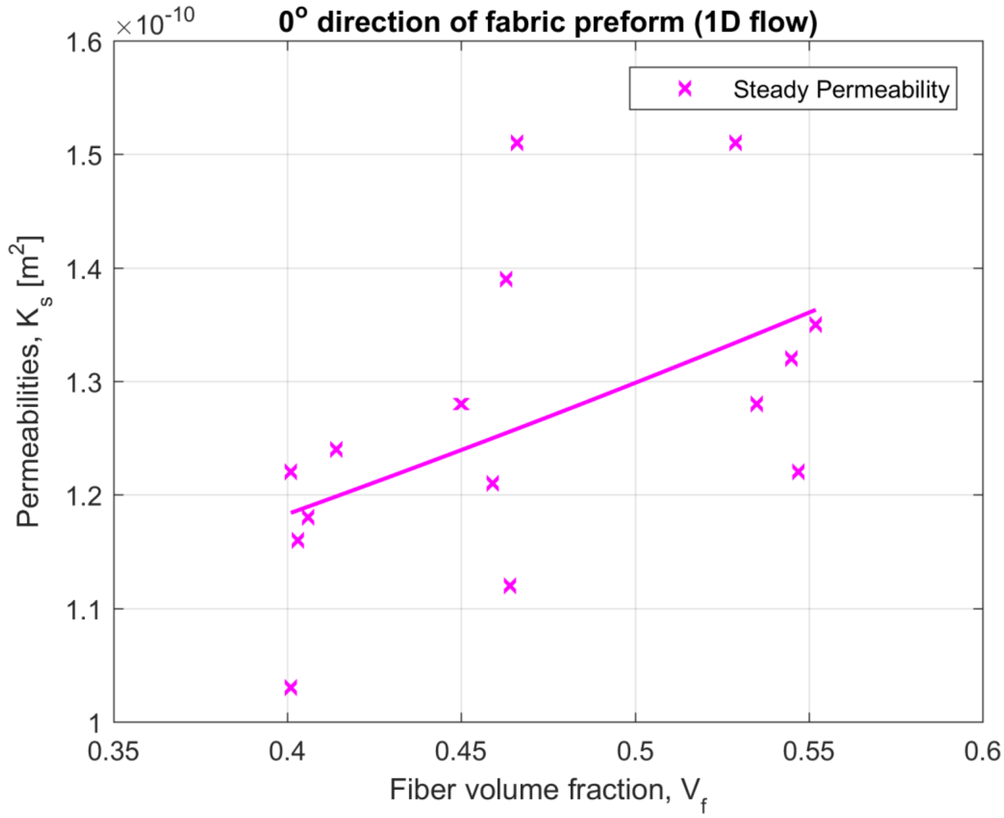

Figure 5.7 Results of 1D steady permeability experiments for 0° direction of fabric preform.

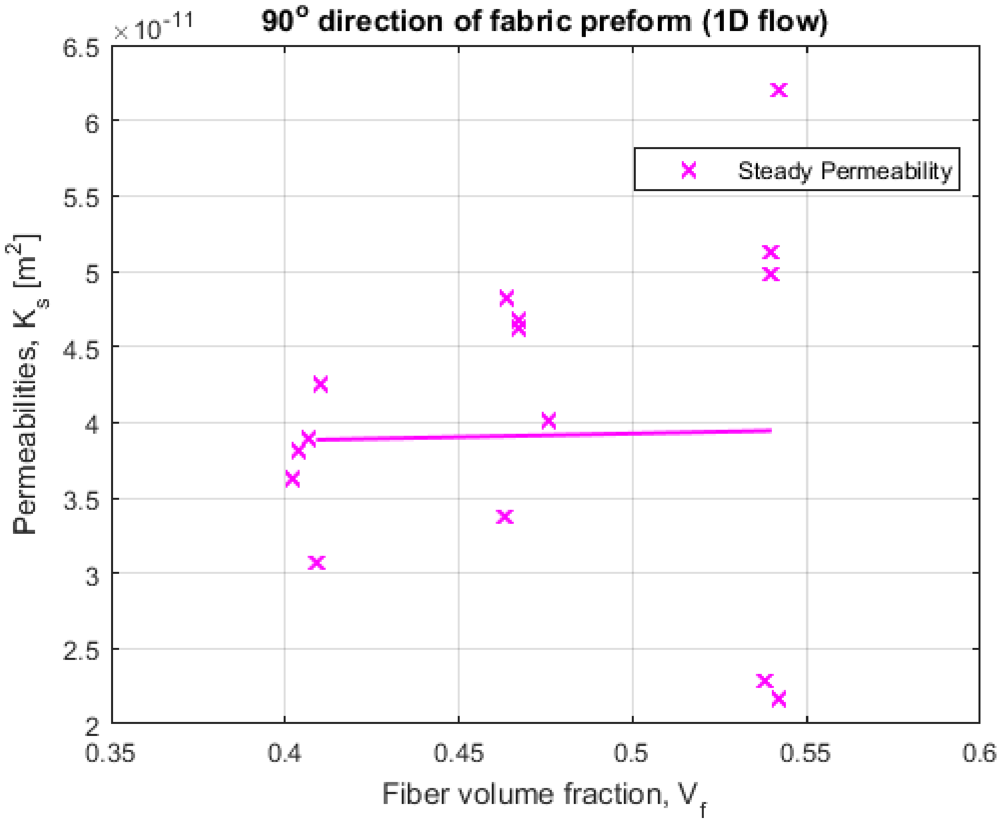

Figure 5.8 Results of 1D steady permeability experiments for 90° direction of fabric preform.

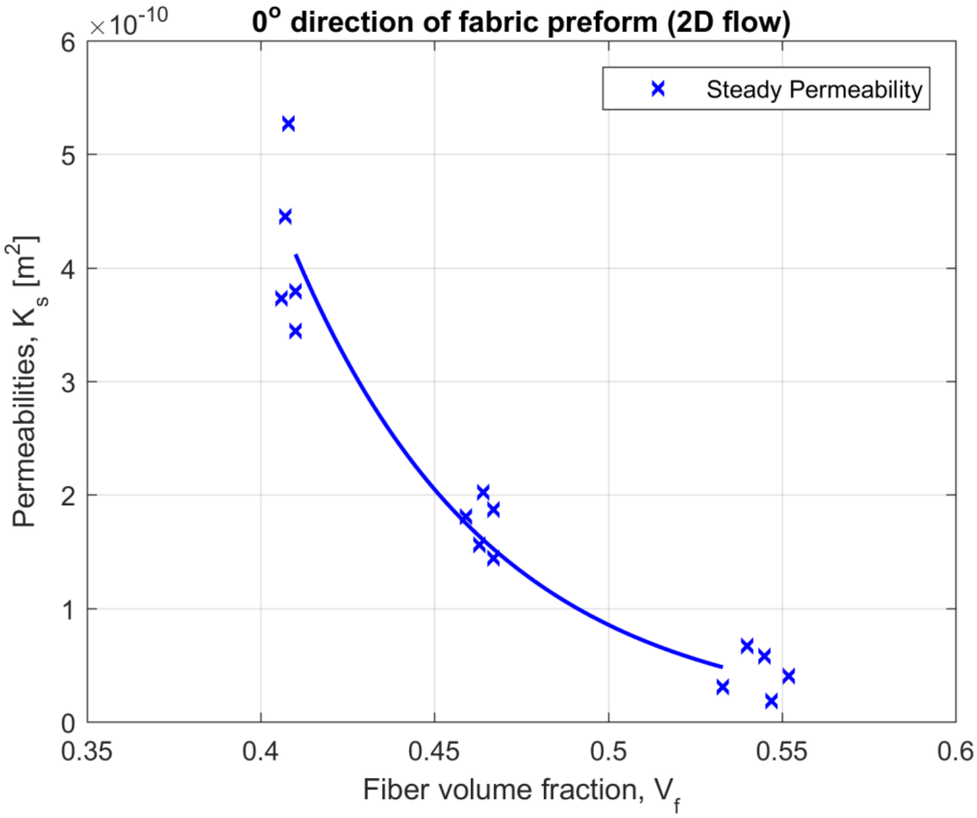

Figure 5.9 Results of 2D steady permeability experiments for 0° direction of fabric preform.

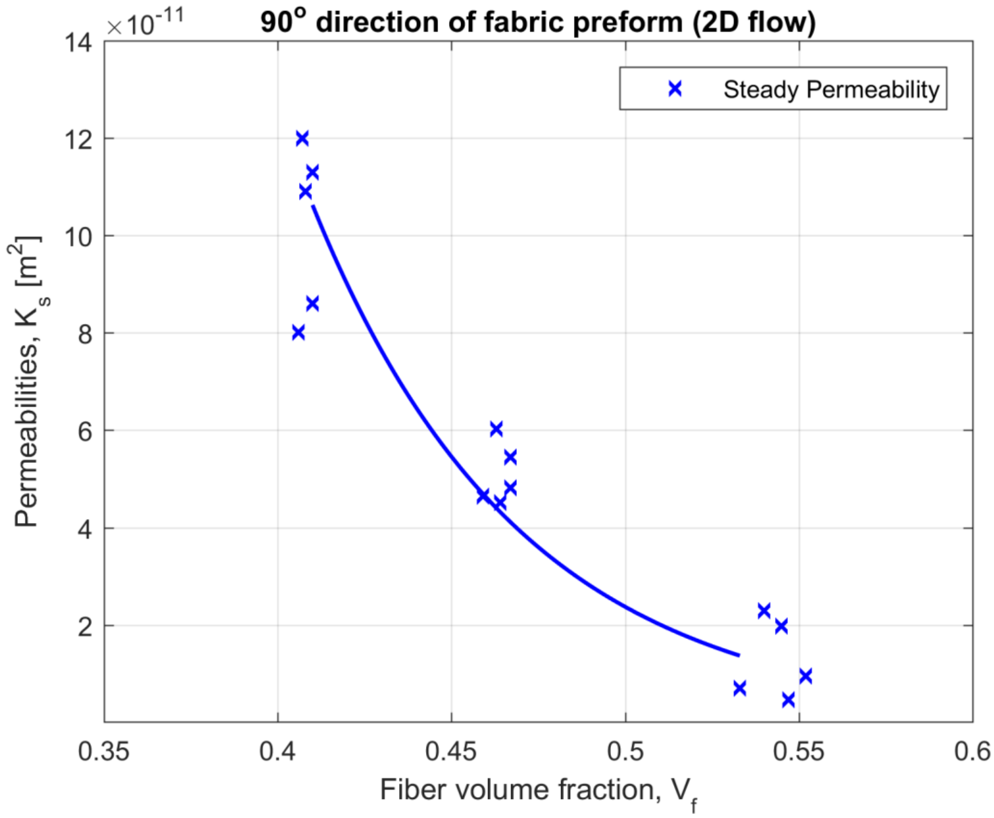

Figure 5.10 Results of 2D steady permeability experiments for 90° direction of fabric preform.

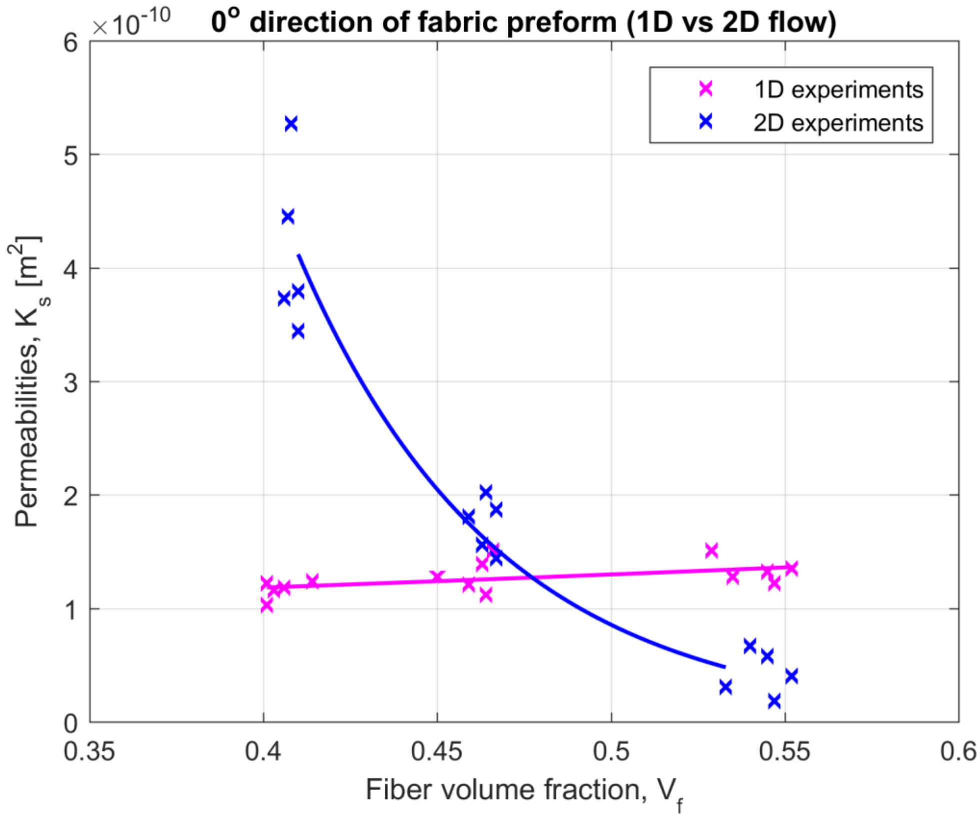

Figure 5.11 Results of 1D and 2D steady permeability experiments for 0° direction of fabric preform.

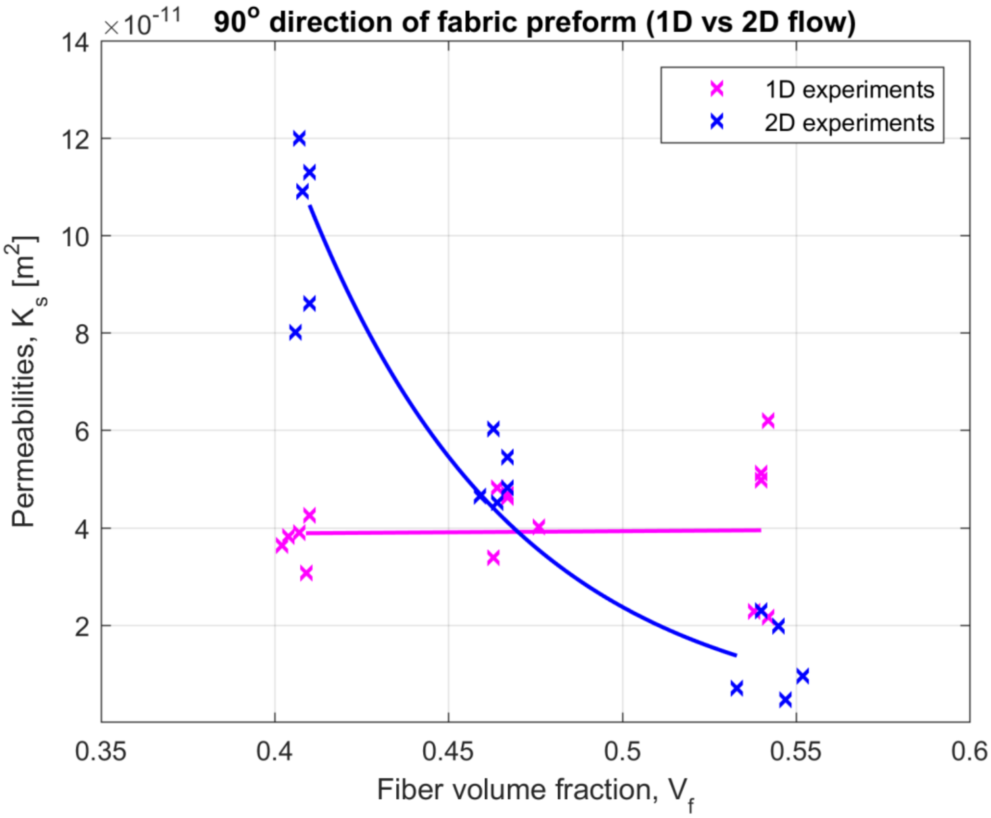

Figure 5.12 Results of 1D and 2D steady permeability experiments for 90° direction of fabric preform.

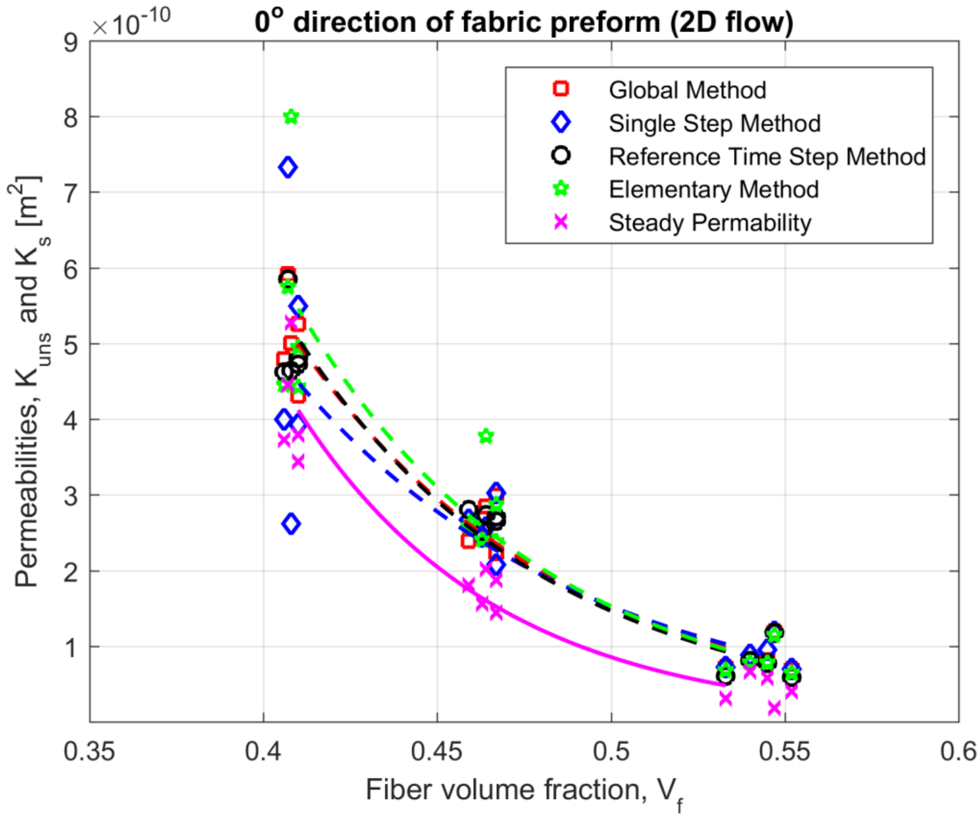

Figure 5.13 Results of 2D permeability experiments for 0° direction of fabric preform.

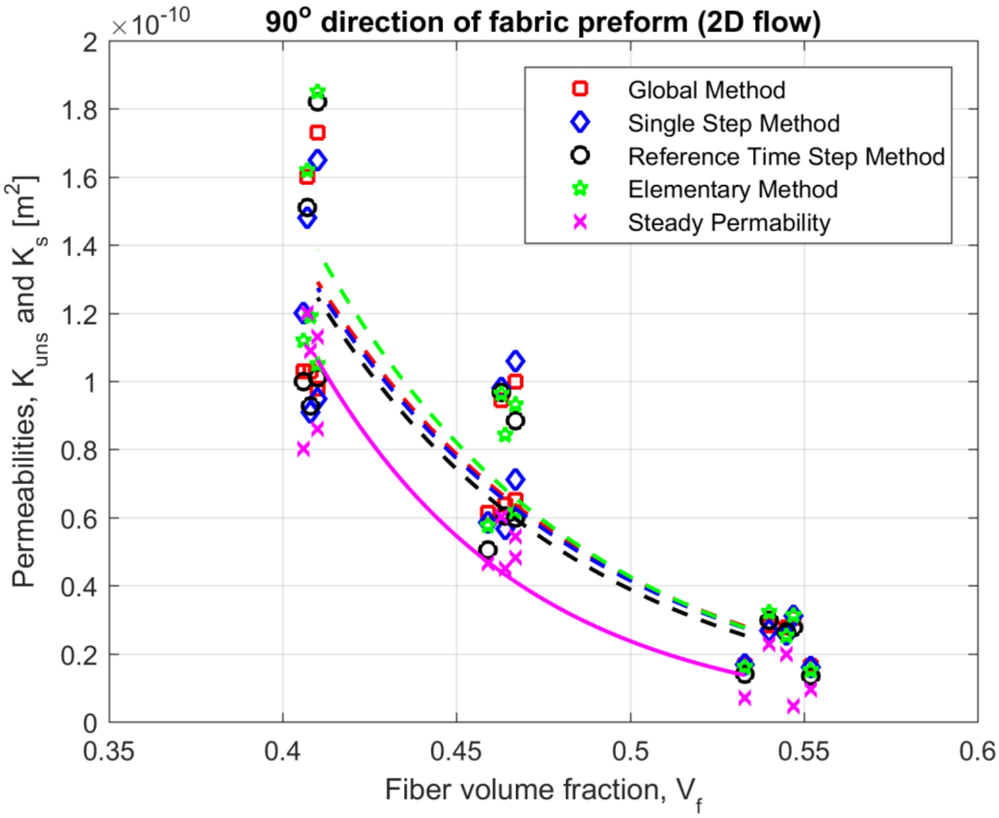

Figure 5.14 Results of 2D permeability experiments for 90° direction of fabric preform.

Table 5.1 Results of 1D unsteady permeability experiments for 0° direction.

	1D flow	$K_{uns,0}$ [m²] (0° direction of fabric preform)					Average [m²]	Standard Deviation [m²]	Variation	Mean R^2
h = 3.00 mm	Global Method	1.92E-10	2.18E-10	1.84E-10	1.88E-10	1.57E-10	1.88E-10	2.18E-11	11.6%	0.999
	Single Step Method	2.43E-10	1.92E-10	1.77E-10	1.80E-10	1.54E-10	1.89E-10	3.31E-11	17.5%	0.990
	Reference Time Step Method	1.90E-10	2.22E-10	2.07E-10	1.78E-10	1.47E-10	1.89E-10	2.87E-11	15.2%	0.996
	Elementary Method	1.92E-10	2.27E-10	1.99E-10	1.90E-10	1.59E-10	1.93E-10	2.43E-11	12.6%	0.999
h = 3.50 mm	Global Method	2.87E-10	2.91E-10	2.95E-10	2.4E-10	2.83E-10	2.792E-10	2.24E-11	8.01%	0.999
	Single Step Method	3.32E-10	3.73E-10	3.99E-10	2.64E-10	3.22E-10	3.38E-10	5.18E-11	15.3%	0.986
	Reference Time Step Method	3.18E-10	3.23E-10	3.03E-10	2.55E-10	2.60E-10	2.918E-10	3.22E-11	11.0%	0.996
	Elementary Method	2.95E-10	3.03E-10	2.98E-10	2.44E-10	2.79E-10	2.838E-10	2.40E-11	8.45%	0.995
h = 4.00 mm	Global Method	2.69E-10	3.24E-10	3.40E-10	3.38E-10	3.22E-10	3.186E-10	2.89E-11	9.06%	0.999
	Single Step Method	2.76E-10	4.13E-10	2.90E-10	3.51E-10	4.13E-10	3.486E-10	6.52E-11	18.7%	0.988
	Reference Time Step Method	2.65E-10	3.73E-10	3.93E-10	3.51E-10	3.57E-10	3.478E-10	4.91E-11	14.1%	0.995
	Elementary Method	2.69E-10	3.37E-10	3.61E-10	3.60E-10	3.35E-10	3.324E-10	3.75E-11	11.3%	0.995

Table 5.2 Results of 1D unsteady permeability experiments for 90° direction.

	1D flow	$K_{uns,90}$ [m²] (90° direction of fabric preform)					Average [m²]	Standard Deviation [m²]	Variation	Mean R^2
h = 3.00 mm	Global Method	6.15E-11	6.24E-11	5.26E-11	5.15E-11	3.97E-11	5.35E-11	9.20E-12	17.2%	0.999
	Single Step Method	6.14E-11	6.17E-11	5.28E-11	4.99E-11	5.23E-11	5.56E-11	5.52E-12	9.93%	0.993
	Reference Time Step Method	6.13E-11	6.19E-11	5.98E-11	5.40E-11	4.36E-11	5.61E-11	7.67E-12	13.7%	0.998
	Elementary Method	6.20E-11	6.47E-11	5.45E-11	5.28E-11	4.71E-11	5.62E-11	7.13E-12	12.7%	0.996
h = 3.50 mm	Global Method	7.00E-11	6.06E-11	7.16E-11	7.12E-11	7.84E-11	7.04E-11	6.37E-12	9.05%	0.999
	Single Step Method	6.71E-11	5.87E-11	6.64E-11	6.78E-11	8.16E-11	6.83E-11	8.28E-12	12.1%	0.999
	Reference Time Step Method	7.88E-11	6.66E-11	7.35E-11	7.20E-11	8.02E-11	7.42E-11	5.48E-12	7.39%	0.998
	Elementary Method	7.20E-11	6.27E-11	7.30E-11	7.21E-11	7.99E-11	7.19E-11	6.12E-12	8.51%	0.999
h = 4.00 mm	Global Method	7.57E-11	9.77E-11	8.45E-11	8.61E-11	6.71E-11	8.22E-11	1.15E-11	14.0%	0.999
	Single Step Method	7.82E-11	1.75E-10	8.39E-11	6.50E-11	6.77E-11	9.40E-11	4.59E-11	48.9%	0.989
	Reference Time Step Method	7.95E-11	1.05E-10	8.35E-11	8.65E-11	6.54E-11	8.40E-11	1.43E-11	17.0%	0.999
	Elementary Method	7.78E-11	1.06E-10	8.66E-11	8.98E-11	6.63E-11	8.53E-11	1.47E-11	17.3%	0.997

Table 5.3 Results of 2D unsteady permeability experiments for 0° direction.

	2D flow	$K_{uns,0}$ [m²] (0° direction of fabric preform)					Average [m²]	Standard Deviation [m²]	Variation	Mean R^2
h = 3.00 mm	Global Method	7.22E-11	7.00E-11	8.14E-11	8.22E-11	1.20E-10	8.52E-11	2.02E-11	23.7%	0.997
	Single Step Method	7.26E-11	7.00E-11	9.54E-11	8.85E-11	1.19E-10	8.91E-11	1.98E-11	22.2%	0.997
	Reference Time Step Method	6.01E-11	5.87E-11	7.76E-11	8.11E-11	1.18E-10	7.91E-11	2.40E-11	30.3%	0.975
	Elementary Method	6.84E-11	6.51E-11	7.85E-11	7.85E-11	1.15E-10	8.11E-11	1.99E-11	24.5%	0.981
h = 3.50 mm	Global Method	2.85E-10	2.39E-10	2.44E-10	2.99E-10	2.23E-10	2.58E-10	3.24E-11	12.5%	0.994
	Single Step Method	2.57E-10	2.67E-10	2.45E-10	3.02E-10	2.08E-10	2.56E-10	3.41E-11	13.3%	0.989
	Reference Time Step Method	2.74E-10	2.80E-10	2.52E-10	2.71E-10	2.65E-10	2.68E-10	1.06E-11	4.0%	0.978
	Elementary Method	3.78E-10	2.58E-10	2.41E-10	2.87E-10	2.38E-10	2.80E-10	5.79E-11	20.7%	0.941
h = 4.00 mm	Global Method	4.31E-10	4.79E-10	5.92E-10	5.00E-10	5.26E-10	5.06E-10	5.96E-11	11.8%	0.964
	Single Step Method	3.93E-10	4.00E-10	7.33E-10	2.62E-10	5.49E-10	4.67E-10	1.80E-10	38.5%	0.911
	Reference Time Step Method	4.80E-10	4.62E-10	5.85E-10	4.64E-10	4.72E-10	4.93E-10	5.21E-11	10.6%	0.952
	Elementary Method	4.43E-10	4.45E-10	5.75E-10	8.00E-10	4.95E-10	5.52E-10	1.49E-10	27.0%	0.912

Table 5.4 Results of 2D unsteady permeability experiments for 90° direction.

	2D flow	$K_{uns,90}$ [m²] (90° direction of fabric preform)					Average [m²]	Standard Deviation [m²]	Variation	Mean R^2
h = 3.00 mm	Global Method	1.67E-11	1.65E-11	2.78E-11	2.83E-11	3.05E-11	2.40E-11	6.80E-12	28.4%	0.997
	Single Step Method	1.69E-11	1.61E-11	2.57E-11	2.67E-11	3.11E-11	2.33E-11	6.54E-12	28.1%	0.993
	Reference Time Step Method	1.40E-11	1.34E-11	2.65E-11	2.98E-11	2.77E-11	2.23E-11	7.92E-12	35.6%	0.979
	Elementary Method	1.40E-11	1.34E-11	2.65E-11	2.98E-11	2.77E-11	2.23E-11	7.92E-12	35.6%	0.975
h = 3.50 mm	Global Method	6.38E-11	6.14E-11	9.44E-11	9.99E-11	6.51E-11	7.69E-11	1.86E-11	24.2%	0.995
	Single Step Method	5.66E-11	5.86E-11	9.81E-11	1.06E-10	7.12E-11	7.81E-11	2.27E-11	29.1%	0.990
	Reference Time Step Method	6.04E-11	5.05E-11	9.67E-11	8.85E-11	5.98E-11	7.12E-11	2.02E-11	28.3%	0.974
	Elementary Method	6.04E-11	5.05E-11	9.67E-11	8.85E-11	5.98E-11	7.12E-11	2.02E-11	28.3%	0.951
h = 4.00 mm	Global Method	9.79E-11	1.03E-10	1.60E-10	1.03E-10	1.73E-10	1.27E-10	3.61E-11	28.3%	0.991
	Single Step Method	9.49E-11	1.20E-10	1.48E-10	9.09E-11	1.65E-10	1.24E-10	3.25E-11	26.2%	0.982
	Reference Time Step Method	1.01E-10	1.00E-10	1.51E-10	9.27E-11	1.82E-10	1.25E-10	3.93E-11	31.3%	0.987
	Elementary Method	1.01E-10	1.00E-10	1.51E-10	1.19E-10	1.85E-10	1.31E-10	3.65E-11	27.8%	0.963

Table 5.5 Results of 1D steady permeability experiments for 0° direction.

1D flow	$K_{s,0}$ [m²] 0° direction of fabric preform)					Average [m²]	Standard Deviation [m²]	Variation
h = 3.00 mm	1.35E-10	1.51E-10	1.28E-10	1.32E-10	1.22E-10	1.34E-10	1.09E-11	8.1%
h = 3.50 mm	1.28E-10	1.21E-10	1.39E-10	1.12E-10	1.51E-10	1.30E-10	1.53E-11	11.7%
h = 4.00 mm	1.03E-10	1.16E-10	1.18E-10	1.24E-10	1.22E-10	1.17E-10	8.23E-12	7.1%

Table 5.6 Results of 1D steady permeability experiments for 90° direction.

1D flow	$K_{s,90}$ [m²] 90° direction of fabric preform)					Average [m²]	Standard Deviation [m²]	Variation
h = 3.00 mm	4.98E-11	6.2E-11	5.12E-11	2.28E-11	2.16E-11	4.15E-11	1.82E-11	43.9%
h = 3.50 mm	3.38E-11	4.82E-11	4.68E-11	4.01E-11	4.62E-11	4.30E-11	6.02E-12	14.0%
h = 4.00 mm	3.63E-11	3.89E-11	3.81E-11	4.25E-11	3.07E-11	3.73E-11	4.32E-12	11.6%

Table 5.7 Results of 2D steady permeability experiments for 0° direction.

2D flow	$K_{s,0}$ [m²] 0° direction of fabric preform)					Average [m²]	Standard Deviation [m²]	Variation
h = 3.00 mm	3.05E-11	4.03E-11	5.79E-11	6.66E-11	1.84E-11	4.27E-11	1.97E-11	46.0%
h = 3.50 mm	2.02E-10	1.81E-10	1.56E-10	1.44E-10	1.87E-10	1.74E-10	2.36E-11	13.6%
h = 4.00 mm	3.79E-11	3.73E-11	4.45E-10	5.27E-10	3.44E-10	2.78E-10	2.29E-10	82.3%

Table 5.8 Results of 2D steady permeability experiments for 90° direction.

2D flow	$K_{s,90}$ [m²] 90° direction of fabric preform)					Average [m²]	Standard Deviation [m²]	Variation
h = 3.00 mm	7.05E-12	9.50E-12	1.98E-11	2.29E-11	4.68E-12	1.28E-11	8.08E-12	63.2%
h = 3.50 mm	4.51E-11	4.65E-11	6.02E-11	4.82E-11	5.45E-11	5.09E-11	6.32E-12	12.4%
h = 4.00 mm	8.60E-11	8.01E-11	1.20E-10	1.09E-10	1.13E-10	1.02E-10	1.75E-11	17.2%

Table 5.9 Results of 2D permeability experiments.

	$K_{uns,0}$ [m^2]	$K_{uns,90}$ [m^2]	μ [Pa.s]	$\dot{m}$ [g/s]	Q [m^3/s]	Length x Width [m x m]	h [m]	$K_{s,0}$ [m^2]	$K_{s,90}$ [m^2]	P_{inj} [kPa]
1	7.22E-11	1.67E-11	0.0974	0.0783	8.12E-08	0.21 x 0.21	0.003	3.05E-11	7.05E-12	79.6
2	7.00E-11	1.65E-11	0.1013	0.1009	1.05E-07	0.21 x 0.21	0.003	4.03E-11	9.50E-12	80.4
3	8.14E-11	2.78E-11	0.0985	0.1712	1.78E-07	0.21 x 0.21	0.003	5.79E-11	1.98E-11	79.7
4	8.22E-11	2.83E-11	0.0982	0.1978	2.05E-07	0.21 x 0.21	0.003	6.66E-11	2.29E-11	79.4
5	1.20E-10	3.05E-11	0.0957	0.0495	5.13E-08	0.21 x 0.21	0.003	1.84E-11	4.68E-12	78.9
6	2.85E-10	6.38E-11	0.0993	0.5814	6.03E-07	0.21 x 0.21	0.0035	2.02E-10	4.51E-11	79.1
7	2.39E-10	6.14E-11	0.1018	0.5391	5.59E-07	0.21 x 0.21	0.0035	1.81E-10	4.65E-11	79.5
8	2.44E-10	9.44E-11	0.0994	0.5602	5.81E-07	0.21 x 0.21	0.0035	1.56E-10	6.02E-11	79.6
9	2.99E-10	9.99E-11	0.0988	0.4904	5.09E-07	0.21 x 0.21	0.0035	1.44E-10	4.82E-11	79.4
10	2.23E-10	6.51E-11	0.0976	0.6138	6.37E-07	0.21 x 0.21	0.0035	1.87E-10	5.45E-11	80.1
11	4.31E-10	9.79E-11	0.0980	1.2602	1.31E-06	0.21 x 0.21	0.004	3.79E-10	8.60E-11	78.6
12	4.79E-10	1.03E-10	0.0967	1.2434	1.28E-06	0.21 x 0.21	0.004	3.73E-10	8.01E-11	78.6
13	5.92E-10	1.60E-10	0.0958	1.6336	1.69E-06	0.21 x 0.21	0.004	4.45E-10	1.20E-10	78.9
14	5.00E-10	1.03E-10	0.0968	1.7146	1.78E-06	0.21 x 0.21	0.004	5.27E-10	1.09E-10	78.6
15	5.26E-10	1.73E-10	0.0973	1.333	1.38E-06	0.21 x 0.21	0.004	3.44E-10	1.13E-10	78.3

5.2. Sample Calculation for 1D (Linear) Permeability Measurement Experiment under Constant Pressure Boundary Condition

Calculation of K_{uns} and K_s permeability values for 0^o direction of fabric preform are illustrated below for mold cavity, h = 3.5 mm.

Input data are listed below:

N = 5	(Number of layers)
m = 123.4	[g], (mass of the fabric preform)
h = 3.50	[mm], (thickness of the fabric preform)
l = 300	[mm], (length of the fabric preform)
w = 100	[mm], (width of the fabric preform)
ρ_{bulk} = 2540	[kg/m^3], (bulk density of glass fiber)
μ = 0.0959	[Pa.s], (viscosity of the resin)
ρ_{resin} = 964	[kg/m^3], (bulk density of glass fiber)
ΔP = 80.0	[kPa], (pressure differential)

The calculations of superficial density (ρ_{sup}), fiber volume fraction(V_f) and porosity (ϕ) are shown below.

$$\rho_{\text{sup}} = \frac{(123.4)}{(5)(0.1)(0.3)} = 823\ g/m^2 \ \text{(per layer)}$$

$$V_f = \frac{N\,\rho_{sup}}{h\,\rho_{bulk}} = \frac{(5)(823)}{(3.5)(2540)} = 0.463 = 46.3\ \%$$

$$\phi = 1 - V_f = 0.537 = 53.7\ \%$$

1D unsteady permeability (K_{uns}) for four different evaluation methods are determined by using the following equation where four different C values are obtained by using four different evaluation methods as explained in Chapter 4.

$$K_{uns,gm} = \frac{C\,\mu\,\phi}{2\,\Delta P} = \frac{(7.945\ x\ 10^{-4})(0.0959)(0.537)}{2(80000)} = 2.56\ x\ 10^{-10}\ m^2$$

$$K_{uns,ssm} = \frac{C\,\mu\,\phi}{2\,\Delta P} = \frac{(7.934\ x\ 10^{-4})(0.0959)(0.537)}{2(80000)} = 2.56\ x\ 10^{-10}\ m^2$$

$$K_{uns,rtsm} = \frac{C\,\mu\,\phi}{2\,\Delta P} = \frac{(8.064\ x\ 10^{-4})(0.0959)(0.537)}{2(80000)} = 2.60\ x\ 10^{-10}\ m^2$$

$$K_{uns,em} = \frac{C\,\mu\,\phi}{2\,\Delta P} = \frac{(8.249\ x\ 10^{-4})(0.0959)(0.537)}{2(80000)} = 2.66\ x\ 10^{-10}\ m^2$$

To calculate 1D steady permeability (K_s) of the fabric preform along 0^o direction, volumetric flow rate Q (negative rate of the change in the inlet reservoir) is obtained by dividing the slope of dm/dt to the density of the resin ρ

$$Q = \frac{1}{\rho}\frac{dm}{dt} = \frac{(1.30\ x\ 10^{-4})}{964} = 1.35\ x\ 10^{-7}\ m^3/s$$

Then, volumetric flow rate Q is used in the following formula

$$K_s = \frac{Q\,\mu\,L}{w\,h\,\Delta P} = \frac{(1.35\ x\ 10^{-7})(0.0959)(0.3)}{(0.1)(0.0035)(80000)} = 1.39\ x\ 10^{-10}\ m^2$$

5.3. Sample Calculation for 2D (Radial) Permeability Measurement Experiment under Constant Pressure Boundary Condition

For the experiment number 1 given in Table 5.9, calculation of K_{uns} and K_s permeability values for 0^o direction of fabric preform are illustrated below.

Input data are listed below:

N = 5	(Number of layers)
m = 179.1	[g], (weight of the fabric preform)
h = 3.00	[mm], (thickness of the fabric preform)
l = 210	[mm], (length of the fabric preform)
w = 210	[mm], (width of the fabric preform)
ρ_{bulk} = 2540	[kg/m^3], (bulk density of glass fiber)
μ = 0.0974	[Pa.s], (viscosity of the resin)
ρ_{resin} = 964	[kg/m^3], (bulk density of glass fiber)
ΔP = 79.6	[kPa], (pressure differential)

The calculations of superficial density (ρ_{sup}), fiber volume fraction(V_f) and porosity (ϕ) are shown below:

$$\rho_{\text{sup}} = \frac{(179.1)}{(5)(0.21)(0.21)} = 812\ g/m^2 \ \text{(per layer)}$$

$$V_f = \frac{N\,\rho_{sup}}{h\,\rho_{bulk}} = \frac{(5)(812)}{(3)(2540)} = 0.533 = 53.3\ \%$$

$$\phi = 1 - V_f = 0.537 = 46.7\ \%$$

2D unsteady permeability ($K_{uns,0}$) for four different evaluation methods are determined by using the following equation. Four different F values are obtained by using four different evaluation methods as explained in Chapter 4.

$$F \equiv K_{uns,0}\, t = \frac{\mu\, \phi}{4P_{inj}} \left\{ r_{f,0}^2 \left(2\, ln\left(\frac{r_{f,0}}{r_i}\right) - 1 \right) + r_i^2 \right\}$$

$$K_{uns,0,gm} = 2.44\, x\, 10^{-10}\, m^2$$

$$K_{uns,0,ssm} = 2.45\, x\, 10^{-10}\, m^2$$

$$K_{uns,0,rtsm} = 2.52\, x\, 10^{-10}\, m^2$$

$$K_{uns,0,em} = 2.41\, x\, 10^{-10}\, m^2$$

Pressure and velocity fields are computed numerically by using the method detailed in Chapter 2, and the results of the experiment number 1, which is given in Table 5. 9, are shown in Fig. 5. 15.

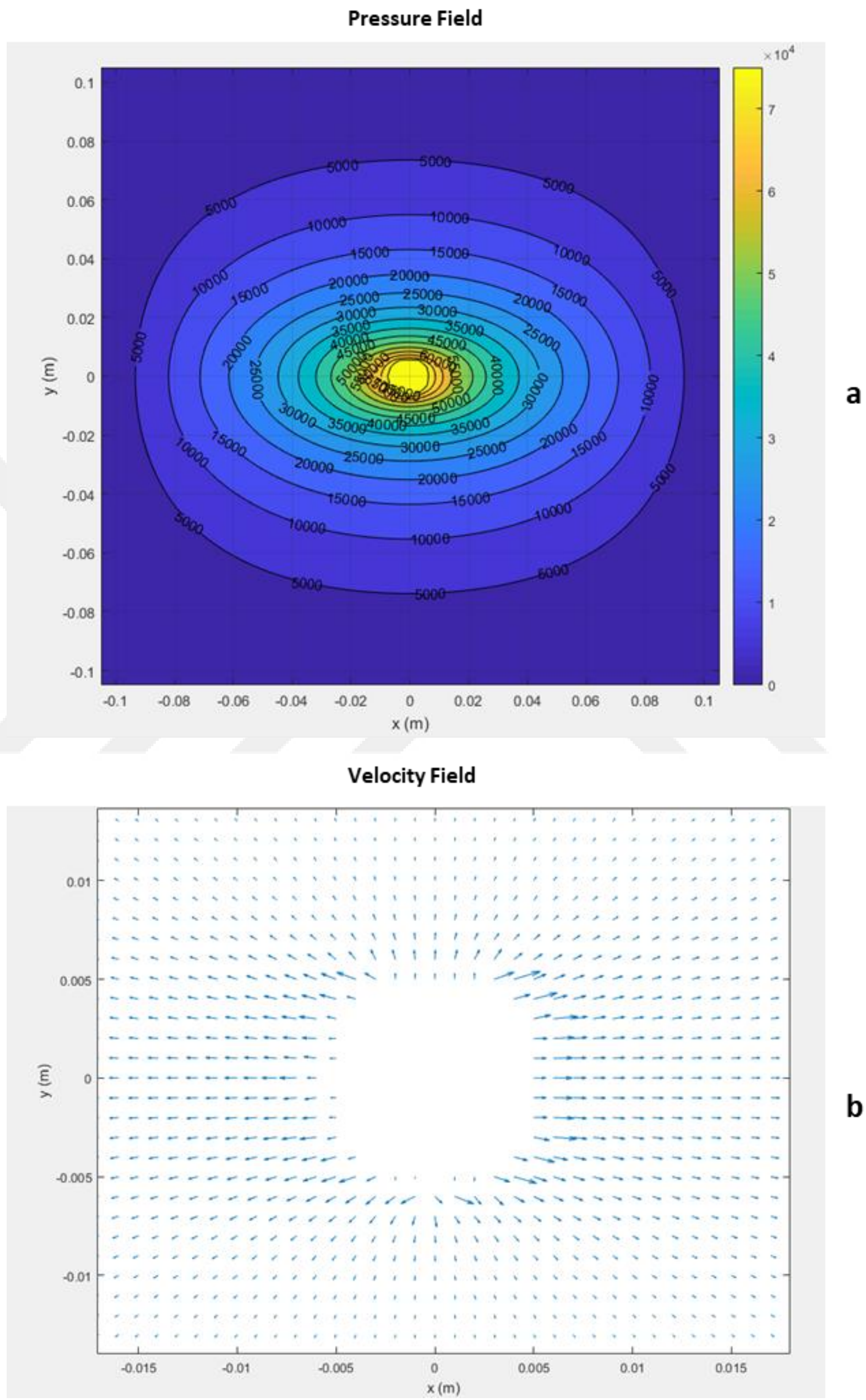

Figure 5.15 Numerically evaluated (a) pressure field and (b) velocity field for experiment 1 in Table 5. 9.

5.4. Sample Calculation for Through-Thickness Permeability Measurement Experiment under Constant Pressure Boundary Condition

K_z permeability values for through-thickness direction of fabric preform are illustrated below.

Input data are listed below:

N = 30 (Number of layers)

m = 94.6 [g], (weight of the fabric preform)

h = 10.0 [mm], (thickness of the fabric preform)

d = 95 [mm], (diameter of the fabric preform)

d_f = 90 [mm], (diameter of the resin flow)

μ = 0.0922 [Pa.s], (viscosity of the resin)

ΔL = 0.49 [m], (height difference between the pressure sensor and top of the exit tube)

ΔP = 96.3 [kPa], (pressure differential) ($\Delta P = P_{inj,gage} - \rho g \Delta L$)

The cross-sectional area, S of the flow channel is calculated as shown below

$$S = \pi(d_f/2)^2 = \pi(0.045^2) = 0.006362\ m^2$$

By using the experimental data of the resin mass accumulated with time in the digital scale, mass flow rate is calculated by fitting a first order curve to the data as shown in Fig. 13. Mass flow rate is divided by the resin density to calculate the volumetric flow rate as detailed above, and the resulting volumetric flow rate is found to be $Q = 1.249\ x\ 10^{-6}\ m^3/s$. The following equation is used for the calculation of the through-thickness permeability

$$K_z = \frac{Q\,\mu\,h}{S\,\Delta P} = \frac{(1.249\,x\,10^{-6})(0.0922)(0.01)}{(0.006362)(96300)} = 1.88\,x\,10^{-12}\,m^2$$

This through-thickness permeability value is one to two orders of magnitude lower than the in-plane permeability values presented in this chapter, which is in agreement with the findings of other researchers in the literature for other fabric types used in LCM processes [16].

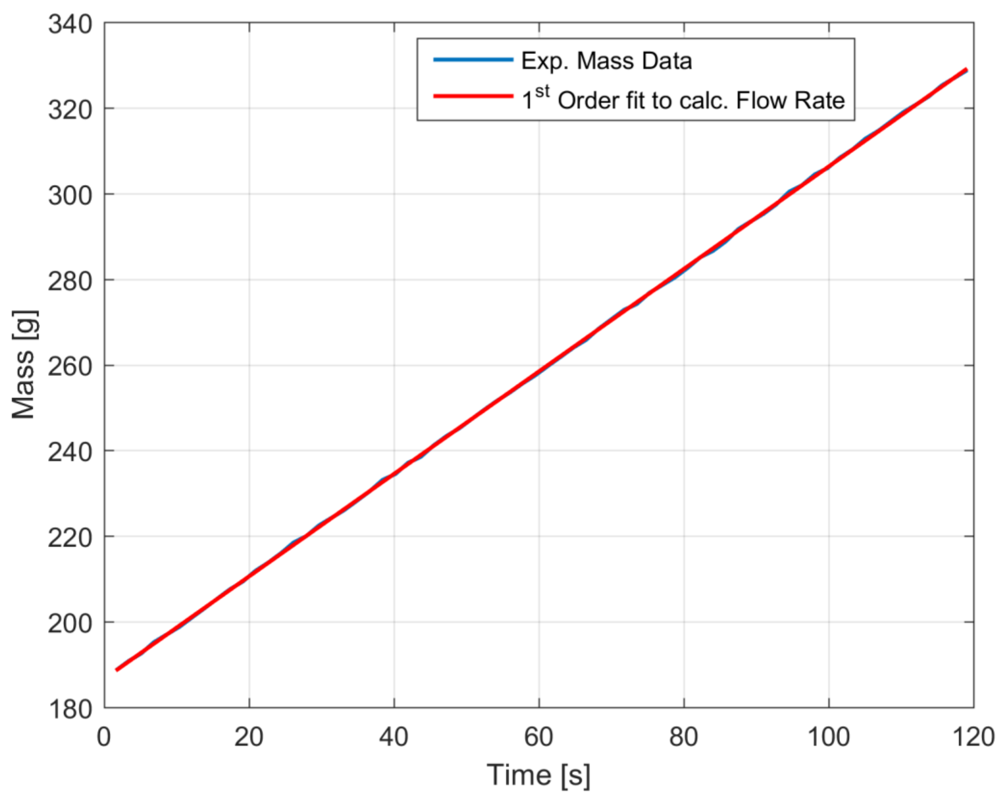

Figure 5.16 Mass of the resin versus time.

Because of the confidentiality agreement, fabric specifications and characterization experimental data are not detailed, but only one sample of through-thickness experiment was demonstrated here in this study.

5.5. Summary, Conclusion and Future Work

The unsteady and steady permeabilities of the biaxial fabric preform under constant-injection pressure boundary condition were measured at different mold cavity thicknesses (h = 3.00 mm, 3.50 mm and 4.00 mm) in different flow dimensions (in-plane 1D, in-plane 2D and through-thickness) by using three experimental setups that were designed and constructed.

Four common curve fitting methods in the literature (global, single-step, reference time step, and elementary methods) were used to fit a best curve to all or some of the experimental data.

For both 1D and 2D unsteady permeability measurements, global method resulted in the highest R^2 values which means that its curve fits represent the results of the experiments better than the other three methods.

The 2D steady permeability of the anisotropic preform was measured numerically by assuming the angle of rotation β is negligible as detailed in Chapter 2. The flow model and its numerical solution allowed to compute the 2D steady permeability components together. This is a novel approach presented here.

The scatter of 1D unsteady permeabilities around a fiber volume fraction is small which may indicate the consistency of the experiments.

Although, one through-thickness permeability experiment with sample calculation is demonstrated in this study, the mold design and experimental procedure help offering a guideline for through-thickness experiment.

As a future work, 1D permeability experimental setup will be modified to have more controllable mold cavity thickness with an extended measurement and adjustment items. Once this is achieved, the 1D unsteady and steady experiments will be repeated. 2D permeability experimental setup will also be modified to track the flow arrival to higher number of locations. In its current state, the 2D permeability setup does not allow to monitor flow front continuously along 0^o, 45^o, 90^o due to the upper mold plate which was designed in a way that it has a high rigidity and thus low deflection.

References

[1] S. G. Advani and E. M. Sozer, "Process Modeling in Composites Manufactoring," p. 436, 2002.

[2] K. Raghu Raja Pandiyan, G. Kundu, S. Neogi, and J. Patel, "Development of Manufacturing Technology for Cab Front Using Resin Transfer Molding Process," *J. Compos. Mater.*, vol. 44, no. 18, pp. 2217–2231, 2010.

[3] A. Sarioglu, "Permeability measurement experiments for fabric preform using LCM processes," 2012.

[4] M. A. Yalcinkaya, B. Caglar, and E. M. Sozer, "Effect of permeability characterization at different boundary and flow conditions on vacuum infusion process modeling," *J. Reinf. Plast. Compos.*, vol. 36, no. 7, pp. 491–504, 2017.

[5] J. R. Weitzenböck, R. A. Shenoi, and P. A. Wilson, "Radial flow permeability measurement. Part A: theory," *Compos. Part A Appl. Sci. Manuf.*, vol. 30, no. 6, pp. 781–796, 1999.

[6] R. Arbter, J. M. Beraud, C. Binetruy, L. Bizet, J. Bréard, S. Comas-Cardona, C. Demaria, A. Endruweit, P. Ermanni, F. Gommer, S. Hasanovic, P. Henrat, F. Klunker, B. Laine, S. Lavanchy, S. V. Lomov, A. Long, V. Michaud, G. Morren, E. Ruiz, H. Sol, F. Trochu, B. Verleye, M. Wietgrefe, W. Wu, and G. Ziegmann, "Experimental determination of the permeability of textiles: A benchmark exercise," *Compos. Part A Appl. Sci. Manuf.*, vol. 42, no. 9, pp. 1157–1168, 2011.

[7] N. Vernet, E. Ruiz, S. Advani, J. B. Alms, M. Aubert, M. Barburski, B.

Barari, J. M. Beraud, D. C. Berg, N. Correia, M. Danzi, T. Delavière, M. Dickert, C. Di Fratta, A. Endruweit, P. Ermanni, G. Francucci, J. A. Garcia, A. George, C. Hahn, F. Klunker, S. V. Lomov, A. Long, B. Louis, J. Maldonado, R. Meier, V. Michaud, H. Perrin, K. Pillai, E. Rodriguez, F. Trochu, S. Verheyden, M. Weitgrefe, W. Xiong, S. Zaremba, and G. Ziegmann, "Experimental determination of the permeability of engineering textiles: Benchmark II," *Compos. Part A Appl. Sci. Manuf.*, vol. 61, pp. 172–184, 2014.

[8] M. A. Yalcinkaya, A. Sarioglu, and E. M. Sozer, "A novel mold design for one-continuous permeability measurement of fiber preforms," *J. Reinf. Plast. Compos.*, vol. 34, no. 11, pp. 915–930, 2015.

[9] M. Akif Yalcinkaya and E. M. Sozer, "Effect of part thickness variation on the mold filling time in vacuum infusion process," *J. Reinf. Plast. Compos.*, vol. 33, no. 23, pp. 2136–2150, 2014.

[10] D. Merhi, V. Michaud, L. Kämpfer, P. Vuilliomenet, and J. A. E. Månson, "Transverse permeability of chopped fibre bundle beds," *Compos. Part A Appl. Sci. Manuf.*, vol. 38, no. 3, pp. 739–746, 2007.

[11] M. Lee, C. B. Park, and C. Tzoganakis, "Measurements and modeling of PS/supercritical CO2 solution viscosities," *Polym. Eng. Sci.*, vol. 39, no. 1, pp. 99–109, 1999.

[12] T. Kimya, M. Odası, and E. Bölge, "This book is published by UCTEA Chamber of Chemical Engineers Bu kitap 2-4 November 2017 2- 4 Kasım 2017 Preparation / Hazırlık Cansu KÖROĞLU UCTEA Chamber of

Chemical Engineers Aegean Branch," no. November, 2017.

[13] P. Ferland, D. Guittard, and F. Trochu, "Concurrent methods for permeability measurement in resin transfer molding," *Polym. Compos.*, vol. 17, no. 1, pp. 149–158, 1996.

[14] A. Colin Cameron and F. A. G. Windmeijer, "An R-squared measure of goodness of fit for some common nonlinear regression models," *J. Econom.*, vol. 77, no. 2, pp. 329–342, 1997.

[15] M. J. Crawley, *The R Book*. 2007.

[16] R. S. Parnas, K. M. Flynn, and M. E. Dal-Favero, "A permeability database for composites manufacturing," *Polym. Compos.*, vol. 18, no. 5, pp. 623–633, 1997.